

The pomeron in diffractive deep inelastic scattering

N. N. Nikolaev

Institut Für Kernphysik (Theorie), KFA Jülich, D-52425 Jülich, Germany and L. D. Landau Institute for Theoretical Physics, 117940 Moscow, Russia

B. G. Zakharov

L. D. Landau Institute for Theoretical Physics, 117940 Moscow, Russia

(Submitted 5 January 1994)

Zh. Eksp. Teor. Fiz. **105**, 1117–1152 (May 1994)

We discuss diffractive deep inelastic scattering at very small x and derive the properties of the diffractive dissociation of virtual photons in the triple-pomeron regime in our technique of the multiparton light cone wave functions. We demonstrate that photon–pomeron interactions can be described by the partonic structure function, which satisfies the QCD evolution equations, and identify the valence and sea (anti)quark and the valence gluon structure functions of the pomeron. The gluon structure function of the pomeron can be described by the constituent gluon wave function of the pomeron. We derive the leading unitarization correction to the rising structure functions at small x and conclude that the unitarized structure function satisfies the linear evolution equations. This result holds even when the multipomeron exchanges are included.

1. INTRODUCTION

The pomeron (IP) remains one of the most mysterious objects in high-energy physics. Apart from elastic scattering, the exchange of pomerons describes (Fig. 1) diffractive dissociation of the projectile, which can be viewed as projectile–pomeron interaction (Fig. 1c).¹ In diffractive leptonproduction at $x=Q^2/(Q^2+W^2)\ll 1$ one can think of deep inelastic scattering (DIS) on the pomeron emitted by the target nucleon.^{2–8} (Here W is the total energy in the photon–proton center of mass system, $W^2=2pq-Q^2$, where p and q are the 4-momenta of the proton and photon, and $Q^2=-q^2$ is the virtuality of the photon.) If diffractive dissociation is dominated by single pomeron exchange, which is a very strong assumption, and if pomeron exchange can be treated as a factorizing particle exchange, which also is a very strong assumption, then one can introduce an operational definition of the (virtual) photon–pomeron cross section $\sigma_{\text{tot}}(\gamma^*\text{IP}, Q^2, M^2)$ and the structure function of the pomeron $F_2^{(\text{IP})}(x, Q^2)$ in terms of the differential cross section $d\sigma_D/dtdM^2$ of the forward diffractive dissociation of virtual photons $\gamma^*+p\rightarrow X+p$ (we follow the Regge theory convention¹ with the substitution $M^2\rightarrow M^2+Q^2$, which is natural for DIS):

$$\sigma_{\text{tot}}(\gamma^*\text{IP}, M^2) = \frac{16\pi}{\sigma_{\text{tot}}(pp)} (M^2 + Q^2) \times \left. \frac{d\sigma_D(\gamma^*+p\rightarrow X+p)}{dtdM^2} \right|_{t=0} \quad (1)$$

and

$$F_2^{(\text{IP})}(x, Q^2) = \frac{Q^2}{4\pi^2\alpha_{em}} \sigma_{\text{tot}}(\gamma^*\text{IP}, M^2), \quad (2)$$

with the corresponding Bjorken variable

$$x = \frac{Q^2}{Q^2 + M^2}. \quad (3)$$

Although there has already been much work on the parton model phenomenology of the pomeron,^{2–10} a definitive proof that the structure function of the pomeron defined in this manner satisfies the conventional Gribov–Lipatov–Dokshitzer–Altarelli–Parisi (GLDAP) QCD evolution equations^{11–13} is as yet lacking. The definition (1) for $\sigma_{\text{tot}}(\gamma^*\text{IP})$ does implicitly assume that the pomeron has the intercept $\alpha_P(0) = 1$, i.e., the high-energy cross sections are constant and the mass spectrum of excitation of large masses M has $1/M^2$ behavior,

$$\frac{1}{\sigma_{\text{tot}}(aN)} \left. \frac{d\sigma_D(a+N\rightarrow X+N)}{dtdM^2} \right|_{t=0} = A_{3\text{IP}} \frac{1}{M^2}. \quad (4)$$

If the factorization relations are valid, then $A_{3\text{IP}}$ is expected to be a universal dimensional constant independent of the projectile a . However, in QCD there are no *a priori* reasons for the factorization relations to hold, and there are indications to the contrary.^{7,8,14,15} Furthermore, factorization can be strongly violated by absorption (unitarity) effects from the multiple pomeron exchanges in Figs. 1b and 1d.⁶ These multiple pomeron exchanges cast doubt on the reinterpretation of diffractive dissociation in terms of photon–pomeron interaction. Experimentally $\alpha_{\text{IP}}(0) > 1$,^{16,17} the total cross sections are rising and the mass spectrum of the diffractive dissociation of protons exhibits slight deviations from a $1/M^2$ law.¹⁸ Furthermore, the cross section for diffractive dissociation of virtual photons was shown to be infrared-sensitive.^{7–9,19} The quantity related to the diffractive dissociation cross section—the unitarization (shadowing, absorption) correction to the structure functions at small x —is also infrared-sensitive.^{19–22} Therefore, the pos-

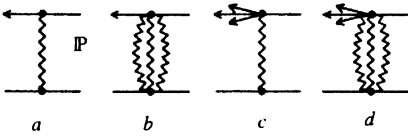


FIG. 1. The single- and multiple-pomeron exchange contributions to the (a,b) elastic scattering and (c,d) the diffraction dissociation amplitudes.

sibility of introducing the well-defined (and well-behaved in the sense of QCD evolution) structure function of the pomeron and the issue of the infrared sensitivity of the diffractive dissociation cross section deserve further study.

In this paper we address the above problems in the context of the light-cone s -channel approach to diffractive DIS at small $x = Q^2/(W^2 + Q^2)$ initiated in our previous publications^{7,23,24} (for related early work on the s -channel approach to light-cone QED see Bjorken, Kogut, and Soper²⁵). Our strategy is to compute the high energy behavior of the total (virtual) photoabsorption cross section and of the diffractive dissociation cross section. We treat diffractive γ^*p scattering in terms of the absorption of the light-cone partonic Fock components of the virtual photon by the target proton or nucleus. One can do so since at $x \ll 1$ the photon transforms into these partonic Fock components at large distances

$$\Delta z \sim \frac{1}{m_N x} \gg R_N, R_A \quad (5)$$

upstream of the target nucleon (nucleus). As an illustration of the principal points of the light-cone formalism,^{24,7} consider interactions of the $q\bar{q}$ Fock state of the photon. Because of the condition (5), the transverse size ρ of the $q\bar{q}$ pair and the partition z and $(1-z)$ of the (light-cone) momentum of the photon between the quark and antiquark can be considered frozen in the scattering process. Therefore, one can introduce a spatial wave function of the light-cone $q\bar{q}$ Fock states $\Psi_{\gamma^*}(\rho, z)$ and the dipole cross section $\sigma(\rho)$ such that the total photoabsorption cross section $\sigma_{T,L}(\gamma^*N, x, Q^2)$ for the (T) transverse and (L) longitudinal photons and the forward diffractive dissociation cross section can be calculated as the conventional quantum mechanical expectation value^{24,7}

$$\sigma_{T,L}(\gamma^*N, x, Q^2) = \int_0^1 dz \int d^2\vec{\rho} |\Psi_{T,L}(z, \rho)|^2 \sigma(\rho), \quad (6)$$

$$\begin{aligned} \left. \frac{d\sigma_D(\gamma^* \rightarrow X)}{dt} \right|_{t=0} &= \int dM^2 \left. \frac{d\sigma_D(\gamma^* \rightarrow X)}{dt dM^2} \right|_{t=0} \\ &= \frac{1}{16\pi} \int_0^1 dz \int d^2\vec{\rho} |\Psi_{T,L}(z, \rho)|^2 \sigma(\rho)^2. \end{aligned} \quad (7)$$

We emphasize that the factorization of the integrands in Eqs. (6, 7) is *exact*, and corresponds to the exact diagonalization of the scattering matrix in the (ρ, z) -representation.

Interactions of the $q\bar{q}$ Fock state of the photon give the driving terms of the structure function at small x and of the diffractive dissociation cross section. Specifically, Eq. (6) yields the photoabsorption cross section and the proton structure function $F_2^{(N)}(x, Q^2)$, which are constant vs x . Equation (7) yields the mass spectrum of the diffractively produced states

$$d\sigma_D(\gamma^* \rightarrow X)/dM^2 \propto 1/(Q^2 + M^2)^2$$

and can be associated with the ‘valence’ $q\bar{q}$ component of the pomeron.^{7,23,24} Both the rise of $F_2^{(N)}(x, Q^2)$ toward small x and the triple-pomeron component of the mass spectrum in the diffractive dissociation of photons, which can be associated with the ‘sea’ $q\bar{q}$ pairs and gluons in the pomeron, are generated by interactions of the higher, $q\bar{q}g_1 \dots g_n$ Fock states of the photon.

The subject of this paper is a generalization of the light-cone s -channel approach^{7,24} to interactions of the higher Fock states of the photon. We derive a full description of diffractive DIS in terms of the generalized dipole cross section. We demonstrate that this dipole cross section satisfies an integral equation, which has as its limiting cases both the Balitskii–Fadin–Kuraev–Lipatov (BFKL) equation^{26–28} and the GLDAP evolution equation.^{11–13} A discussion of the BFKL limit of our equation is presented elsewhere;²⁹ in this paper we concentrate on the GLDAP limit or the Double-Leading Logarithm Approximation (DLA).

Our major findings can be summarized as follows. The diffractive dissociation cross section can indeed be factorized [Eq. (94)] into the flux of pomerons in the proton $f_{\text{IP}}(y)/y$, where $y = (M^2 + Q^2)/(W^2 + Q^2)$ is a fraction of proton’s (light-cone) momentum carried by the emitted pomeron, and the well-defined structure function of the pomeron $F_2^{(\text{IP})}(x/y, Q^2)$, which undergoes conventional QCD evolution with Q^2 [the definition (1) corresponds to the convention $f_{\text{IP}}(y) = 1$]. This structure function and the flux of pomerons describe how the naive $\propto 1/M^2$ mass spectrum (4) is modified by rising hadronic cross sections and by QCD evolution effects. The factorization (94) shows a certain resemblance to the usual Regge theory factorization, despite the fact that the Regge theory factorization relations do not hold in DIS at small x , and in our analysis we never assume or use the Regge theory factorization. We speak of the triple pomeron regime just to pay tribute to the fact that we mostly consider $Q^2 \ll M^2 \ll W^2$, which in Regge theory would have been the triple pomeron domain. The infrared sensitivity of the diffractive dissociation cross section can be reabsorbed into the initial momentum distribution of the ‘constituent’ quarks, antiquarks and gluons in the pomeron, in close similarity to the conventional QCD evolution analysis of the proton structure function. We demonstrate that besides the ‘valence’ and ‘sea’ quark–antiquark components derived in,⁷ the pomeron has a ‘valence’ gluon component, and present the explicit derivation of the constituent gluon wave function of the pomeron. The absolute normalization of the pomeron structure function can be related to the triple-pomeron coupling $A_{3\text{IP}}(Q^2)$ Eq. (62), which gives the

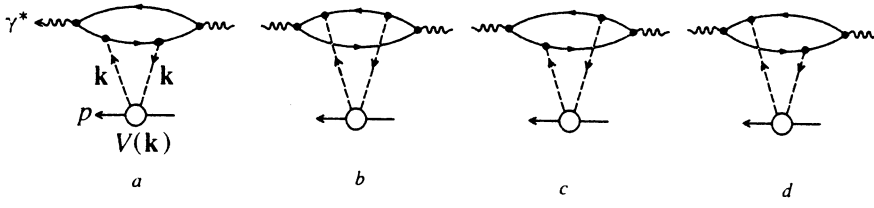


FIG. 2. The lowest-order QCD diagrams for interaction of the $q\bar{q}$ Fock state of the photon with the target nucleon. In all the figures the wavy, solid and dashed lines are for the photon, (anti)quarks and gluons, respectively.

driving term of the diffractive dissociation mass spectrum (4). We shall confirm the earlier suggestion³⁰ that despite being dimensional quantity, $A_{3\text{IP}}(Q^2) \propto \text{GeV}^{-2}$, this triple-pomeron coupling only has weak dependence on Q^2 , although if $1/\sqrt{Q^2}$ were the only relevant scale in the DIS, then naively one could have expected $A_{3\text{IP}}(Q^2) \propto 1/Q^2$. The fact that one can (approximately) relate the properties of diffractive dissociation in DIS and in real photoabsorption, which here is proven rather than assumed, is interesting in and of itself. In Ref. 7 we gave a phenomenological estimate of the sea structure function of the pomeron and of the diffractive dissociation rate in terms of the triple-pomeron coupling $A_{3\text{IP}}(0)$ derived from real photo-production data.³¹ The resulting predictions are in good agreement with the first data on the diffractive dissociation of photons in DIS at HERA obtained recently by the ZEUS collaboration.³²

Diffractive dissociation of virtual photons and unitarity (shadowing, absorption) corrections to the rising structure functions at small x are two closely related phenomena. s -channel unitarization of the virtual photoabsorption cross section introduces multiple-pomeron exchanges, which could lead to the departure of the x - and Q^2 -dependence of the structure function from the predictions of GLDAP evolution. We find that the unitarity corrections are large and persist at all Q^2 . The unitarity correction is a nonlinear functional of the parton density, and violates the conventional linear relationship between the photoabsorption cross section and the parton density. Our principal conclusion is that the modified evolution equations nonetheless retain their linear GLDAP form as distinct from the nonlinear equation suggested in Ref. 19 and discussed extensively in the literature over the past decade (for a recent review with many references, see Ref. 22). The diagonalization of the scattering matrix in our $(\vec{\rho}, z)$ representation^{7,24} greatly simplifies a discussion of the unitarization correction, as it enables one to unambiguously identify the s -channel partial waves which must satisfy the unitarity bound.

This paper is organized as follows. In Sec. 2 we review the light-cone s -channel approach to DIS starting with diffractive interactions of the two-body $q\bar{q}$ Fock state of the photon.^{7,24} In Sec. 3 we study interactions of the 3-body $q\bar{q}g$ Fock state of the photon and derive the driving term of the triple-pomeron mass spectrum in the diffractive dissociation of virtual photons and the driving term of the sea structure function of the pomeron. In Sec. 4 we apply our formalism to derivation of the rising structure function in the DLLA. Here the generalized dipole cross section emerges as the principal quantity which controls the dif-

fractive DIS. We demonstrate that the dipole cross section satisfies the generalized BFKL equation. The subject of Sec. 5 is the triple-pomeron regime of diffractive dissociation of photons to higher orders in perturbative QCD. Here we derive the structure function and the constituent gluon wave function of the pomeron. The latter absorbs the infrared regularization dependence of the diffractive dissociation cross section. This completes a derivation⁷ of the valence and sea (anti)quark and the gluon structure functions of the pomeron, which are to be used as an input of the GLDAP evolution of the pomeron structure function. The factorization properties of the QCD pomeron and the flux of pomerons in the proton are discussed in Sec. 6. In Sec. 7 we discuss the unitarization of the rising structure functions of the proton at small x . We demonstrate that the unitarized structure functions of the proton still satisfy the linear GLDAP evolution equations, as distinct from the nonlinear Gribov–Levin–Ryskin (GLR) equations.¹⁹ Remarkably, this conclusion of the linear GLDAP evolution holds even when multiple pomeron exchanges are included. In this section we also present a brief phenomenology of the shadowing correction to the proton structure function and comment on the treacherous path to the interpretation of shadowing in terms of the fusion of partons. Our main results are summarized in Sec. 8.

This paper is mostly devoted to the derivation of the formalism; numerical results are presented in Ref. 33.

2. DIS IN TERMS OF THE FOCK STATES OF THE PHOTON AND THE DIPOLE CROSS SECTION

2.1. The $q\bar{q}$ Fock states of the photon and sea quarks in the proton.

We are interested in DIS at $x \ll 1$, where the structure functions are dominated by the scattering of photons by the sea quarks. The driving term of the sea is given by the perturbative QCD diagrams shown in Fig. 2. The same diagrams can be viewed as scattering of the $q\bar{q}$ Fock states of the photon by the target proton. The principal finding of Ref. 24 is that the corresponding contribution to the photoabsorption cross section can be cast in the quantum mechanical form (6). The wave functions of the $q\bar{q}$ fluctuations of the photon were derived in Ref. 24, and read

$$|\Psi_T(z, \rho)|^2 = \frac{6\alpha_{em}}{(2\pi)^2} \sum_1^{N_f} Z_f^2 \{ [z^2 + (1-z)^2] \varepsilon^2 K_1(\varepsilon\rho)^2 + m_f^2 K_0(\varepsilon\rho)^2 \}, \quad (8)$$

$$|\Psi_L(z, \rho)|^2 = \frac{6\alpha_{em}}{(2\pi)^2} \sum_1^{N_f} 4Z_f^2 Q^2 z^2 (1-z)^2 K_0(\varepsilon\rho)^2, \quad (9)$$

where the $K_\nu(x)$ are modified Bessel functions and

$$\varepsilon^2 = z(1-z)Q^2 + m_f^2. \quad (10)$$

In Eqs. (8)–(10), m_f is the quark mass and z is the Sudakov variable, i.e., the fraction of a photon's light-cone momentum q_- carried by one of the quarks of the pair ($0 < z < 1$). In the diagrams of Fig. 2, the color-singlet $q\bar{q}$ interacts with the target nucleon via the Low–Nussinov³⁴ two-gluon exchange, which is the driving term of the QCD pomeron. The interaction cross section for the color dipole of size ρ is given by²⁴

$$\sigma(\rho) = \frac{16}{3} \alpha_S(\rho) \int \frac{d^2\vec{k} V(k) [1 - \exp(i\mathbf{k}\boldsymbol{\rho})]}{(\mathbf{k}^2 + \mu_G^2)^2} \alpha_S(\mathbf{k}^2). \quad (11)$$

In (11), \mathbf{k} is the transverse momentum of the exchanged gluons, the longitudinal momentum of the exchanged gluons is $\sim m_N x$ and is negligible at small x , and $\mu_G \approx 1/R_c$ is some kind of effective mass of gluons introduced so that color forces do not propagate beyond the confinement radius $R_c \sim R_N$. The gluon–gluon–nucleon vertex function $V(\mathbf{k})$ is related to the two-quark form factor of the nucleon $G_2(\mathbf{k}_1, \mathbf{k}_2) = \langle N | \exp[i(\mathbf{k}_1 \cdot \mathbf{r}_1 + \mathbf{k}_2 \cdot \mathbf{r}_2)] | N \rangle$ by

$$V(k) = 1 - G_2(\mathbf{k}, -\mathbf{k}) \approx 1 - \mathcal{F}_{ch}(3\mathbf{k}^2), \quad (12)$$

where $\mathcal{F}_{ch}(q^2)$ is the charge form factor of the proton. $\alpha_S(k^2)$ is the running QCD coupling which we shall use both in the momentum and coordinate representations:

$$\alpha_S(k^2) = \frac{4\pi}{\beta_0 \log(k^2/\Lambda_{\text{QCD}}^2)}, \quad (13)$$

$$\alpha_S(\rho) = \frac{4\pi}{\beta_0 \log(1/\Lambda^2 \rho^2)},$$

where Λ and Λ_{QCD} may be slightly different: $\Lambda = \Lambda_{\text{QCD}}/C$ with $C \sim 1.5$.²⁴ In the integrand of Eq. (11), the strong coupling $\alpha_S(k^2)$ is understood to be $\min\{\alpha_S(k^2), \alpha_S(\rho)\}$.

2.2. Universality of the dipole cross section and infrared regularization.

The salient feature of the dipole cross section (11) is its universality property.^{7,8} $\sigma(\rho)$ depends only on the size ρ of the $q\bar{q}$ color dipole. The dependence on Q^2 and the quark flavor is concentrated in the wave functions (8) and (9). The fundamental role of color gauge invariance must be emphasized. By virtue of color gauge invariance, gluons of wavelength $\lambda = 1/k > R_N$ decouple from the color-singlet nucleon. This decoupling is taken care of by the vertex function $V(k)$, which vanishes as $k \rightarrow 0$, and the size of the nucleon emerges as a natural infrared regularization: the dipole cross section (11) is infrared-finite even if $\mu_G = 0$. Similarly, the factor $[1 - \exp(i\mathbf{k}\boldsymbol{\rho})]$ takes care of the decoupling of gluons with $\lambda > \rho$ from the color-singlet $q\bar{q}$

Fock state. As a result, at small ρ the cross section $\sigma(\rho)$ is perturbatively calculable with its absolute normalization. For the nucleon target

$$\begin{aligned} \sigma(\rho) &\approx \frac{4\pi}{3} \rho^2 \alpha_S(\rho) \int_0^{1/\rho^2} \frac{dk^2 k^2 V(k)}{(\mathbf{k}^2 + \mu_G^2)^2} \alpha_S(\mathbf{k}^2) \\ &= \frac{16\pi^2}{3\beta_0} \rho^2 \alpha_S(\rho) \log \left[\frac{1}{\alpha_S(\rho)} \right] \\ &= C_N \rho^2 \alpha_S(\rho) L(\rho), \end{aligned} \quad (14)$$

where

$$L(\rho) = \log \left[\frac{1}{\alpha_S(\rho)} \right] \quad (15)$$

is the large parameter of the so-called Leading-Log Approximation (LLA).¹¹

Another universal feature of $\sigma(\rho)$ is its saturation at $\rho > R_N, R_c$ because of confinement.²⁴ This is a strong-coupling regime, and in the saturation regime $\sigma(\rho)$ depends on the infrared regularizations. [Following Gribov,³⁵ we assume freezing-in of strong coupling $\alpha_S(\rho) = \alpha_S(R_f) \sim 1$ at $\rho > R_f$.] One natural infrared regularization—the size of the target proton—enters via the vertex function $V(k)$. The other two infrared regularizations are the effective confinement radius R_c , which enters via the effective gluon mass μ_G , and the freezing point R_f of the strong coupling $\alpha_S(R_f) \sim 1$. Evidently, by virtue of Eq. (6), the dependence on these infrared regularizations propagates into the proton structure function. Here we would like to emphasize that such an infrared sensitivity of $F_2^{(N)}(x, Q^2)$ is old news: in the conventional QCD-improved parton model, this dependence is hidden in the parameterization of the input parton distributions at the low factorization scale Q_0^2 . In our light-cone s -channel approach, we instead calculate the structure function in terms of the dipole cross section, drastically reducing the number of infrared parameters. Furthermore, a crude test of the large- ρ behavior of the dipole cross section $\sigma(\rho)$ is provided by the hadronic cross sections. For instance, the pion–nucleon total cross section can be evaluated as

$$\sigma_{\text{tot}}(\pi N) = \int_0^1 dz \int d^2\rho |\Psi_\pi(z, \rho)|^2 \sigma(\rho), \quad (16)$$

which roughly reproduces the observed value of $\sigma_{\text{tot}}(\pi N)$ at moderate energies.^{7,8,14,15,30} Once the constraint (16) has been enforced, the predictions for DIS to a large extent become parameter-free. Such a minimal-regularization approach leads to a viable description of the absolute value of $F_2^{(N)}(x, Q^2)$,^{23,24,33,36} of the longitudinal structure function $F_L(x, Q^2)$,³⁷ of the nuclear shadowing in DIS^{23,24,36}, of the gluon distribution in the proton,³⁸ and of the excitation of charm in muon and neutrino scattering,³⁹ and roughly reproduces the total cross section of real photoabsorption.^{7,8} Whether the large- r behavior of the dipole cross section $\sigma(r)$ contains the nonperturbative component or not, and what is a magnitude of this component, remains somewhat of an open issue. There is good reason to believe, though,

that the energy dependence of the dipole cross section and the x -dependence of structure functions, which are our major concerns in this paper, must come from the exchange by perturbative gluons, to which our formalism is applicable.

2.3. Connection with the QCD evolution equations.

At small Q^2 , the transverse size of the $q\bar{q}$ Fock states of the photon is given by the Compton wavelength of the quark $1/m_f$. For the heavy flavors (charm,...) this is the perturbatively small size. For the light flavors it is also natural to ask that quarks not propagate beyond the confinement radius. With the natural choice $m_{u,d} \sim \mu_\pi \sim 1/R_c$, Eq. (6) with the wave function (8) reproduces the real photoabsorption cross section.^{7,8} At larger $Q^2 \gg m_f^2, \mu_G^2, R_N^{-2}$, the conventional QCD-improved parton model description is recovered. Indeed, let us calculate the Q^2 dependence of the cross section (6). At large Q^2 , the leading contribution to $\sigma_T(\gamma^*N)$ comes from the $K_1(\varepsilon\rho)^2$ term in Eq. (8). Making use of the properties of the modified Bessel functions, after integrating over z one can write

$$\begin{aligned} \sigma_T(\gamma^*N, x, Q^2) &= \int_0^1 dz \int d^2\rho |\Psi_T(z, \rho)|^2 \sigma(\rho) \\ &\propto \frac{1}{Q^2} \int_{1/Q^2}^{1/m_f^2} \frac{d\rho^2}{\rho^4} \sigma(\rho) \\ &\propto \frac{1}{Q^2} \int_{1/Q^2}^{1/m_f^2} \frac{d\rho^2}{\rho^2} \alpha_S(\rho) \log \left[\frac{1}{\alpha_S(\rho)} \right] \\ &\propto \frac{1}{Q^2} \frac{1}{2!} L(Q^2)^2. \end{aligned} \quad (17)$$

We find the scaling cross section $\propto 1/Q^2$ times the LLA scaling violation factor, with one power of $L(Q^2) = \log[1/\alpha_S(Q^2)]$ per QCD loop, which is the starting point of the derivation¹¹⁻¹³ of the QCD evolution equations. Notice that the factor $1/Q^2$ in Eq. (17), which provides the Bjorken scaling, comes from the probability of having the $q\bar{q}$ fluctuation of the highly virtual photon. There is a finite (and also scaling) contribution to σ_T from the region $\rho^2 < 1/Q^2$:

$$\begin{aligned} \Delta\sigma_T(\rho^2 < 1/Q^2, x, Q^2) &\propto \int_0^{1/Q^2} \frac{d\rho^2}{\rho^2} \sigma(\rho) \\ &\propto \int_0^{1/Q^2} d\rho^2 \alpha_S(\rho) L(\rho) \\ &\propto \frac{1}{Q^2} \alpha_S(Q^2) L(Q^2). \end{aligned} \quad (18)$$

This is the $\sim \alpha_S(Q^2)/L(Q^2)$ correction to the LLA cross section (17). Notice the strong ordering in the LLA cross section:

$$1/Q^2 < \rho^2 < 1/m_f^2. \quad (19)$$

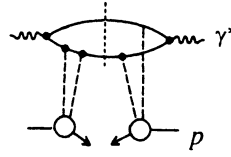


FIG. 3. One of the 16 lowest-order QCD diagrams for the inclusive cross section for forward diffraction dissociation of the $q\bar{q}$ Fock state of the photon. The vertical dashed lines show the unitarity cut corresponding to the diffractively excited state.

The QCD scaling violations are (logarithmically) dominated by $\rho^2 \sim 1/Q^2$. Similar analysis gives the longitudinal cross section

$$\begin{aligned} \sigma_L(\gamma^*N, x, Q^2) &= \int_0^1 dz \int d^2\rho |\Psi_L(z, \rho)|^2 \sigma(\rho) \\ &\propto \frac{1}{Q^4} \int_{1/Q^2}^{1/m_f^2} \frac{d\rho^2}{\rho^6} \sigma(\rho) \\ &\propto \frac{1}{Q^4} \int_{1/Q^2}^{1/m_f^2} \frac{d\rho^2}{\rho^4} \alpha_S(\rho) \log[1/\alpha_S(\rho)] \\ &\propto \frac{1}{Q^2} \alpha_S(Q^2) L(Q^2), \end{aligned} \quad (20)$$

which is completely dominated by $\rho^2 \sim 1/Q^2$ (for more discussion on this point, see Ref. 39).

2.4. Diffraction excitation of the $q\bar{q}$ Fock state of the photon and the 'valence' $q\bar{q}$ component of the pomeron.

The shape of the mass spectrum from the diffraction excitation of the $q\bar{q}$ Fock state of the photon (Fig. 3) can be estimated by undoing the z integration in Eq. (7). Firstly, we note that the diffraction dissociation cross section is dominated by large $\rho^2 \sim R_c^2, m_f^{-2}$ (Ref. 7):

$$\begin{aligned} \left. \frac{d\sigma_{D,T}(\gamma^* \rightarrow X)}{dt} \right|_{t=0} &= \frac{1}{16\pi} \int_0^1 dz \int d^2\rho |\Psi_T(z, \rho)|^2 \sigma(\rho)^2 \\ &\propto \frac{1}{Q^2} \int d\rho^2 \left[\frac{\sigma(\rho)}{\rho^2} \right]^2 \exp(-2m_f\rho) \\ &\propto \frac{1}{Q^2} \int_{1/m_f^2}^{1/Q^2} d\rho^2 \propto \frac{1}{Q^2 m_f^2}. \end{aligned} \quad (21)$$

Secondly, the invariant mass squared of the $q\bar{q}$ system equals

$$M^2 = \frac{\mathbf{k}_q^2 + m_f^2}{z(1-z)}, \quad (22)$$

where \mathbf{k}_q is the transverse momentum of the (anti)quark of the pair. For the crude estimation of the mass spectrum at $M^2 > Q^2$, one can undo the z integration in (7) and (21) by making use of $k^2 \sim 1/\rho^2 \sim m_f^2$, so that $M^2 \sim 1/z\rho^2$ and

$$dz \sim \frac{1}{\rho^2} \frac{dM^2}{M^4}, \quad (23)$$

which gives (for a more detailed derivation see Ref. 7)

$$\begin{aligned} \left. \frac{d\sigma_{D,T}(\gamma^* \rightarrow X)}{dM^2 dt} \right|_{t=0} &\propto \frac{1}{(Q^2 + M^2)^2} \int_0^{1/m_f^2} d\rho^2 \\ &\propto \frac{1}{m_f^2 (Q^2 + M^2)^2}. \end{aligned} \quad (24)$$

Notice the strong flavor dependence of the diffraction dissociation cross section, Eqs. (21) and (24). For the excitation of heavy flavors the diffraction dissociation cross section is perturbatively calculable; for the excitation of light flavors it is evidently infrared-regularization dependent. (We shall encounter such an infrared-regularization sensitivity of the diffraction dissociation cross section over and over again. We shall demonstrate, however, that this infrared sensitivity can be reabsorbed into the normalization of the input structure function of the pomeron, which by itself will be proven to satisfy the GLDAP evolution.) The corresponding contribution to the structure function of the pomeron has a form⁷ reminiscent of the valence structure function of the proton:

$$\begin{aligned} F_2^{(IP)}(x, Q^2) &= \frac{4Q^2}{\pi \alpha_{em} \sigma_{tot}(pN)} (M^2 + Q^2) \\ &\times \left. \frac{d\sigma_D(\gamma^* \rightarrow q + \bar{q})}{dt dM^2} \right|_{t=0} \propto x(1-x). \end{aligned} \quad (25)$$

(The convention (1) for the photon-pomeron cross section differs from that used in Ref. 7 by the factor $(M^2 + Q^2)/M^2$.) Therefore, the diffraction excitation of the $q\bar{q}$ Fock state of the photon can be associated with DIS on the 'valence' $q\bar{q}$ component of the pomeron.

2.5. Rising structure functions and higher Fock states of the photon.

The diagrams of Fig. 2 can also be reinterpreted as Bethe-Heitler production of a $q\bar{q}$ pair by the photon-gluon fusion $\gamma^* g \rightarrow q\bar{q}$. The conventional Weizsäcker-Williams formula for this Bethe-Heitler cross section reads

$$\begin{aligned} \Delta\sigma_{tot}(\gamma^* N, W^2, Q^2) &= \sum_1^{N_f} \int_x^1 dy g(y, Q^2) \sigma \\ &\times (\gamma^* g \rightarrow q_f \bar{q}_f, y W^2), \end{aligned} \quad (26)$$

where $g(y, Q^2)$ is the distribution function of the physical, transverse, gluons in the proton. By the kinematics of DIS,

$$y = \frac{(kq)}{(pq)} = \frac{(M^2 + Q^2)}{(W^2 + Q^2)}. \quad (27)$$

The diagram of Fig. 2 describes the driving term of the perturbative gluon distribution in the proton, which is assumed here to be entirely of radiative origin. At $x \ll 1$, we have^{38,40}

$$g(x, Q^2) = \frac{8}{x} \int_0^{Q^2} \frac{dk^2 k^2}{(k^2 + \mu_G^2)^2} V(k) \frac{\alpha_S(k^2)}{2\pi}. \quad (28)$$

Here it is worthwhile to emphasize that the flux of soft gluons depends only on the color charge, and neither the spin nor the helicity, of the source of gluons. The vertex function $V(k)$ in the integrand of (28) is precisely the same as in Eq. (11) and describes the destructive interference of gluons radiated by different quarks bound in the color-singlet nucleon. In terms of the mass M of the excited $q\bar{q}$ pair, Eqs. (26) and (28) give

$$\Delta\sigma_{tot}(\gamma^* N, W^2, Q^2) \propto \int_{4m_f^2}^{W^2} \frac{dM^2}{Q^2 + M^2} \sigma(\gamma^* g \rightarrow q\bar{q}, M^2). \quad (29)$$

Because of the spin- $\frac{1}{2}$ exchange in the t -channel, the cross section of the photon-gluon fusion subprocess decreases at large M^2 ,

$$\sigma(\gamma^* g \rightarrow q\bar{q}, M^2) \propto \frac{1}{Q^2 + M^2} \log\left(\frac{Q^2 + M^2}{4m_f^2}\right); \quad (30)$$

the integral (29) converges at finite $M^2 \sim Q^2$ and yields a constant photoabsorption cross section at small x . For a closely related reason, one finds the rapidly convergent mass spectrum (24). On the other hand, if the $q\bar{q}g$ final state is produced in the photon-gluon fusion, then because of the spin-1 gluon exchange in the t -channel, $\sigma(\gamma^* g \rightarrow q\bar{q}g, M^2) \propto \text{const}$, which leads to a rising $[\propto \log(1/x)]$ contribution to the photoabsorption cross section.⁴ Notice that excitation of the $q\bar{q}g$ final state in photon-gluon fusion can be reinterpreted as scattering on the nucleon of the $q\bar{q}g$ Fock state of the photon. Therefore, one has to study the effect of higher Fock states of the photon.

3. INTERACTIONS OF THE $q\bar{q}g$ FOCK STATE OF THE PHOTON

3.1. Interaction cross section for the $q\bar{q}g$ state.

One can easily write down the interaction cross section for the color-singlet three-parton $q\bar{q}g$ state using only color gauge invariance considerations (the separation of partons in impact parameter space is shown in Fig. 4):

$$\sigma_3(r, R, \rho) \stackrel{0}{\approx} [\sigma(R) + \sigma(\rho)] - \frac{1}{8}\sigma(r). \quad (31)$$

Indeed, when the separation of the quark and antiquark is small, $r \ll \rho \approx R$, the $q\bar{q}$ pair will be indistinguishable from the pointlike color-octet charge. In this limit

$$\sigma_3(0, \rho, \rho) = \frac{2}{3}\sigma(\rho), \quad (32)$$

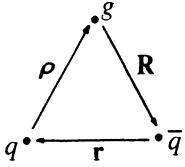


FIG. 4. Spatial structure of the $q\bar{q}g$ Fock state in the impact-parameter plane.

where $9/4$ is the familiar ratio of the octet and triplet strong couplings. In the opposite limiting cases of $R=0$ or $\rho=0$, a gluon and (anti)quark with vanishing separation are indistinguishable from a pointlike (anti)quark and

$$\sigma_3(r,0,r) = \sigma_3(r,r,0) = \sigma(r). \quad (33)$$

The formal derivation goes as follows. In the integrand of the cross section (11), the two propagators $1/(\mathbf{k}^2 + \mu_G^2)$ correspond to the Fourier transforms

$$U(\mathbf{k}) = \int d^3r \exp(-i\mathbf{k}\mathbf{r}) \exp(-\mu_G r)/r$$

and $U(-\mathbf{k})$ of the (infrared-regulated) gluonic Coulomb potential. If the color charge is located at position \mathbf{c} , then $U(\mathbf{k},\mathbf{c}) = U(\mathbf{k})\exp(-i\mathbf{k}\mathbf{c})$. Whenever the two exchanged gluons couple to the same parton, one gets the square of the corresponding strong charge. If the gluons couple to the two partons located at points \mathbf{r}_1 and \mathbf{r}_2 , the corresponding contribution acquires the extra phase factor $\exp[i\mathbf{k}(\mathbf{r}_2 - \mathbf{r}_1)]$. This is precisely the origin of the factor $[1 - \exp(i\mathbf{k}\mathbf{r})]$ in the integrand of Eq. (11). Accurate calculation of color traces for the different couplings of the two exchanged gluons to the quark, antiquark and gluon of the $q\bar{q}g$ Fock state leads precisely to the cross section (31).

If $\Phi_1(\mathbf{r},\mathbf{R},\rho,z,z_g)$ is the wave function of the $q\bar{q}g$ Fock state, the corresponding contribution to $\sigma_{\text{tot}}(\gamma^*p)$ is

$$\Delta\sigma_{\text{tot}}(q\bar{q}g,x,Q^2) = \int dz_g d^2\rho d^2z_g |\Phi_1(\mathbf{r},\mathbf{R},\rho,z,z_g)|^2 \sigma(r,R,\rho). \quad (34)$$

The gluon of the $q\bar{q}g$ Fock state is generated radiatively from the primary $q\bar{q}$ Fock state (Fig. 5), and this radiation simultaneously renormalizes the weight of the $q\bar{q}$ component of the photon. If $n_g(z,\mathbf{r})$ is the number of gluons in the $q\bar{q}g$ state with $q-\bar{q}$ separation \mathbf{r} (we suppress the subscripts T and L in $|\Psi(z,\mathbf{r})|^2$), defined by

$$\int dz_g d^2\rho |\Phi_1(\mathbf{r},\mathbf{R},\rho,z,z_g)|^2 = n_g(z,\mathbf{r}) |\Psi(z,\mathbf{r})|^2, \quad (35)$$

the wave function of the radiationless $q\bar{q}$ component of the photon will renormalize as

$$|\Psi_{q\bar{q}}(z,\mathbf{r})|^2 = |\Psi(z,\mathbf{r})|^2 [1 - n_g(z,\mathbf{r})]. \quad (36)$$

It is convenient to introduce

$$\Delta\sigma(r,R,\rho) = \sigma_3(r,R,\rho) - \sigma(r) = \frac{9}{8} [\sigma(R) + \sigma(\rho) - \sigma(r)], \quad (37)$$

which shows how much the interaction cross section of the $q\bar{q}g$ Fock state is different from the cross section for the $q\bar{q}$ state. Then $\sigma_{\text{tot}}(\gamma^*N)$ from interactions of the $q\bar{q}$ and $q\bar{q}g$ Fock states of the photon takes the form

$$\begin{aligned} \sigma_{\text{tot}}(\gamma^*N,x,Q^2) &= \int dz d^2r |\Psi(z,\mathbf{r})|^2 [1 - n_g(z,\mathbf{r})] \sigma(r) \\ &+ \int dz d^2r dz_g \rho |\Phi_1(\mathbf{r},\mathbf{R},\rho,z,z_g)|^2 \\ &\times [\sigma(r) + \Delta\sigma(r,R,\rho)] \\ &= \int dz d^2r |\Psi(z,\mathbf{r})|^2 \sigma(r) \\ &+ \int dz d^2r dz_g \rho |\Phi_1(\mathbf{r},\mathbf{R},\rho,z,z_g)|^2 \\ &\times \Delta\sigma(r,R,\rho). \end{aligned} \quad (38)$$

Up to now we have manipulated the formally divergent quantity $n_g(z,\mathbf{r})$ as if it were finite. As a matter of fact, the renormalization (36) of the radiationless $q\bar{q}$ Fock state corresponds to the introduction of the so-called regularized splitting functions¹³ in the GLDAP evolution equations, and takes care of the virtual radiative corrections [a very detailed discussion of the interplay of the virtual and real radiative corrections and the emergence of the running strong coupling was given by Dokshitzer¹² (see also the review in Ref. 41), and need not be repeated here]. Of course, the final result for the physical cross section, the last line of Eq. (38), does not contain any divergences.

3.2. Wave function of the $q\bar{q}g$ state and the rising photoabsorption cross section.

We are interested in the $\propto \log(1/x)$ component of the increase in the photoabsorption cross section

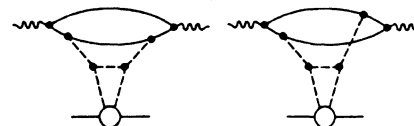


FIG. 5. Scattering of the $q\bar{q}g$ Fock state of the photon on the nucleon by interaction of its radiatively generated gluon.

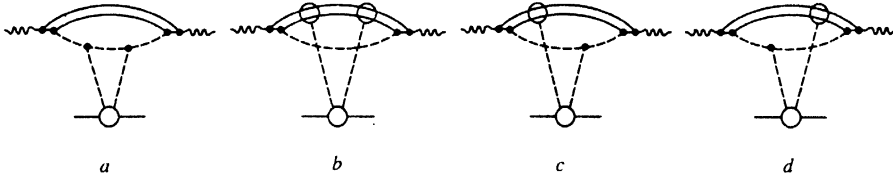


FIG. 6. Different couplings of the exchanged gluons to the color-octet $q\bar{q}$ pair and the gluon of the $q\bar{q}g$ Fock state of the photon.

$$\Delta\sigma_{\text{tot}}^{(1)}(\gamma^*N, x, Q^2) = \int dz d^2r dz_g d^2\rho |\Phi_1(\mathbf{r}, \mathbf{R}, \boldsymbol{\rho}, z, z_g)|^2 \Delta\sigma(r, R, \rho). \quad (39)$$

This $\log(1/x)$ comes from the dz_g/z_g integration in the domain $x < z_g < 1$, and we must concentrate on $z_g \ll 1$. One should not confuse the Sudakov variable z_g , which is the fraction of the light-cone momentum of the photon carried by the gluon, with y , which is the fraction of the light-cone momentum of the proton carried by the same gluon. The two quantities are related by

$$z_g y = x. \quad (40)$$

Only the diagrams of Fig. 6a in which the exchanged gluons couple to the gluon of the $q\bar{q}g$ Fock state give rise to $\Delta\sigma_{\text{tot}}(\gamma^*N, x, Q^2) \propto \log(1/x)$. The corresponding wave function can be reconstructed from the number of gluons n_g in the $q\bar{q}g$ state, which on the one hand equals

$$n_g = \int dz_g d^2\rho dz d^2\mathbf{r} |\Phi_1(\mathbf{r}, \mathbf{R}, \boldsymbol{\rho}, z, z_g)|^2 \quad (41)$$

and, on the other hand, can be evaluated from the Weizsäcker-Williams formula (28),

$$n_g = \frac{2}{3} \cdot \frac{8}{\pi} \int \frac{dz_g}{z_g} \int dz d^2\mathbf{r} |\Psi(\mathbf{r}, z)|^2 \times \int \frac{d^2\mathbf{k}_g k_g^2}{(\mathbf{k}_g^2 + \mu_G^2)^2} \frac{\alpha_S(k_g^2)}{2\pi} [1 - \exp(i\mathbf{k}_g \mathbf{r})]. \quad (42)$$

Here we have used the fact that for the $q\bar{q}$ source of gluons

$$V(\mathbf{k}_g) = \int dz d^2\mathbf{r} |\Psi(\mathbf{r}, z)|^2 [1 - \exp(i\mathbf{k}_g \mathbf{r})], \quad (43)$$

and the factor $2/3$ accounts for the two (anti)quarks in the $q\bar{q}$ state compared to the three quarks in the proton. Transformation of Eq. (42) into the configuration-space integral can easily be performed making use of²⁴

$$\int \frac{d^2\mathbf{k} k^2}{(\mathbf{k}^2 + \mu_G^2)^2} = \int d^2\rho \mu_G^2 K_1(\mu_G \rho)^2 \quad (44)$$

and

$$\int \frac{d^2\mathbf{k} k^2}{(\mathbf{k}^2 + \mu_G^2)^2} \exp(i\mathbf{k} \mathbf{r}) = \int d^2\rho \mu_G^2 K_1(\mu_G \rho) K_1(\mu_G R) \frac{\mathbf{R} \rho}{R \rho}, \quad (45)$$

which yields

$$n_g = \frac{4}{3\pi^2} \int \frac{dz_g}{z_g} d^2\rho \int dz d^2\mathbf{r} |\Psi(\mathbf{r}, z)|^2 \alpha_S(r) \times \mu_G^2 \left| K_1(\mu_G \rho) \frac{\rho}{\rho} - K_1(\mu_G R) \frac{\mathbf{R}}{R} \right|^2. \quad (46)$$

After a more careful treatment of the running coupling, we can identify the three-parton wave function

$$|\Phi_1(\mathbf{r}, \mathbf{R}, \boldsymbol{\rho}, z, z_g)|^2 = \frac{1}{z_g} \frac{1}{3\pi^3} |\Psi(z, r)|^2 \mu_G^2 \times \left| g_S(r_1^{(\min)}) K_1(\mu_G \rho_1) \frac{\rho}{\rho} - g_S(r_2^{(\min)}) K_1(\mu_G R) \frac{\mathbf{R}}{R} \right|^2. \quad (47)$$

Here $g_S(r)$ is the running color charge, $\alpha_S(r) = g_S(r)^2/4\pi$, and the arguments of the color charges are $r_1^{(\min)} = \min\{r, \rho\}$ and $r_2^{(\min)} = \min\{r, R\}$. The wave function (47) has the $1/z_g$ behavior needed for the $\propto \log(1/x)$ rise in the cross section. The color gauge invariance property of the wave function (47) is noteworthy: because of cancellations of the color charges of the quark and antiquark in the color singlet state, it vanishes when $(R - \rho) \rightarrow 0$. It counts only physical, transverse gluons. For those reasons and because of the related color gauge invariance properties of $\sigma(r, R, \rho)$, our introduction of the infrared regularization and the modeling of the confinement by the effective mass of gluons exchanged in the t -channel is consistent with color gauge invariance.

In the DLLA, the leading contribution to $\Delta\sigma_{\text{tot}}^{(1)}(\gamma^*N, x, Q^2)$ comes from the LLA ordering of sizes

$$\frac{1}{Q^2} \ll r^2 \ll \rho^2 \ll R_N^2, \frac{1}{\mu_G^2}, \quad (48)$$

when

$$\mu_G^2 \left| K_1(\mu_G \rho) \frac{\rho}{\rho} - K_1(\mu_G R) \frac{\mathbf{R}}{R} \right|^2 = \frac{r^2}{\rho^2 R^2} \approx \frac{r^2}{\rho^4}, \quad (49)$$

which produces the factorized wave function

$$|\Phi_1(r, R, \rho)|^2 = \frac{1}{z_g} |\Psi(z, r)|^2 \frac{4}{3\pi^2} \alpha_S(r) \frac{r^2}{\rho^4}. \quad (50)$$

Naturally, the LLA wave function (50) does not depend on the infrared regularization parameter μ_G . In the LLA

$$\Delta\sigma(r, R, \rho) = \Sigma(\rho) = \frac{9}{4} \sigma(\rho), \quad (51)$$

and the increase in the total cross section can be written as

$$\begin{aligned} \Delta\sigma_{\text{tot}}(\gamma^* N, x, Q^2) &= \int dz d^2\mathbf{r} |\Psi(z, r)|^2 \alpha_S(r) r^2 \\ &\times \frac{4}{3\pi} \int_x^z \frac{dz_g}{z_g} \int_{\rho^2} \frac{d\rho^2}{\rho^4} \Sigma(\rho) \\ &= \int dz d^2\mathbf{r} |\Psi(z, r)|^2 \alpha_S(r) C_N r^2 \frac{9}{4} \frac{4}{3\pi} \\ &\times \log\left(\frac{z}{x}\right) \int_{\rho^2} \frac{d\rho^2}{\rho^4} \rho^2 \alpha_S(\rho) L(\rho) \\ &= \int dz d^2\mathbf{r} |\Psi(z, r)|^2 \sigma(r) \frac{12}{\beta_0} \cdot \frac{1}{2!} L(r) \\ &\times \frac{1}{1!} \log\left(\frac{z}{x}\right) \propto \frac{1}{Q^2} L(Q)^3 \log\left(\frac{1}{x}\right). \quad (52) \end{aligned}$$

Here we have made explicit use of the small- r behavior of $\sigma(r)$, Eq. (14). This is the first instance when we encounter the expansion parameter of the DLLA^{12,26,41}

$$\xi(x, r) = \frac{12}{\beta_0} L(r) \log\left(\frac{1}{x}\right). \quad (53)$$

We have one power of $L(Q)$ per QCD loop [which a *posteriori* justifies LLA ordering (48)] and one power of $\log(1/x)$ per gluon in the Fock state of the photon.

3.3. The triple-pomeron asymptotics of the mass spectrum of diffraction dissociation.

Our starting point is the generic formula (7). Repeating the considerations of Section 3.2, we can write

$$\begin{aligned} &16\pi \left. \frac{d\sigma_D(\gamma^* \rightarrow q\bar{q} + q\bar{q}g)}{dt} \right|_{t=0} \\ &= 16\pi \int dM^2 \left. \frac{d\sigma_D(\gamma^* \rightarrow q + q\bar{q}g)}{dt dM^2} \right|_{t=0} \\ &= \int dz d^2\mathbf{r} |\Psi(z, r)|^2 [1 - n_g(\mathbf{r})] \sigma(r)^2 \\ &\quad + \int dz d^2\mathbf{r} dz_g d^2\boldsymbol{\rho} |\Phi_1(\mathbf{r}, \mathbf{R}, \boldsymbol{\rho}, z, z_g)|^2 \\ &\quad \times [\sigma(r) + \Delta\sigma(r, R, \rho)]^2 \\ &= \int dz d^2\mathbf{r} |\Psi(z, r)|^2 \sigma(r)^2 \\ &\quad + \int dz d^2\mathbf{r} dz_g d^2\boldsymbol{\rho} |\Phi_1(\mathbf{r}, \mathbf{R}, \boldsymbol{\rho}, z, z_g)|^2 \\ &\quad \times [\Delta\sigma(r, R, \rho)^2 + 2\sigma(r)\Delta\sigma(r, R, \rho)]. \quad (54) \end{aligned}$$

The first term in the last line of Eq. (54) describes the diffraction excitation of the $q\bar{q}$ Fock states into low masses $M^2 \sim Q^2$; see Eq. (24). The second term gives rise to the $1/M^2$ mass spectrum, which can be seen as follows. The invariant mass squared of the $q\bar{q}g$ state equals

$$M^2 = \frac{m_f^2 + k_q^2}{z} + \frac{m_f^2 + k_{\bar{q}}^2}{1-z-z_g} + \frac{k_g^2}{z_g}. \quad (55)$$

Anticipating the final results, we note that the leading contribution to the diffraction dissociation cross section comes from the slightly modified LLA ordering

$$\frac{1}{Q^2} \ll r^2 \ll \rho^2 \sim R_N^2, \frac{1}{\mu_G^2}, \quad (56)$$

i.e., from $Q^2 \gg k_q^2, k_{\bar{q}}^2 \gg k_g^2 \sim \mu_G^2$. Therefore, the excitation of masses $M^2 \gg Q^2$ only comes from $z_g \ll z < 1$, and the dz_g integration in (54) can easily be transformed into the dM^2 integration [see Eqs. (27) and (40)]:

$$\frac{dM^2}{M^2 + Q^2} = \frac{dy}{y} = \frac{dz_g}{z_g}, \quad (57)$$

where now y is the fraction of proton's momentum carried by the pomeron. The wave function (47) has precisely the needed $\propto 1/z_g$ behavior, and [in view of (56) the term $\propto \sigma(r)\Delta\sigma(r, R, \rho)$ in (54) can be neglected] leads to

$$\left. \frac{d\sigma_D}{dt dM^2} \right|_{t=0} = \frac{1}{M^2 + Q^2} \int dz d^2\mathbf{r} |\Psi(z, r)|^2 \alpha_S(r) r^2 C_N \cdot \frac{1}{C_N} \\ \times \frac{1}{16\pi} \cdot \frac{4}{3\pi} \cdot \int_{\rho^2}^{\infty} d\rho^2 \left[\frac{\Sigma(\rho)}{\rho^2} \right]^2 F(\mu_G \rho), \quad (58)$$

where the form factor $F(\mu_G \rho)$ is defined by a slight generalization of (49) to allow for $\mu_G \rho \sim 1$:

$$\mu_G^2 \left| K_1(\mu_G \rho) \frac{\rho}{\rho} - K_1(\mu_G R) \frac{R}{R} \right|^2 = \frac{r^2}{\rho^4} F(\mu_G \rho). \quad (59)$$

The form factor $F(x)$ satisfies $F(0) = 1$ and $F(x) \propto \exp(-2x)$ at $x > 1$.

Firstly, we notice that the diffraction dissociation cross section depends on the infrared regularization, since the ρ integration in (58) is essentially flat and is dominated by large $\rho \sim R_N$, $1/\mu_G$. Then can take $\rho^2 = 0$ for the lower limit of integration, and $d\sigma_D/dt dM^2$ in Eq. (58) factorizes into the Q^2 -independent dimensional constant

$$A_{3IP}^* = \frac{1}{C_N} \cdot \frac{1}{12\pi^2} \cdot \left(\frac{9}{4}\right)^2 \int d\rho^2 \left[\frac{\sigma(\rho)}{\rho^2} \right]^2 F(\mu_G \rho) \quad (60)$$

and the cross section

$$\sigma^*(Q^2) = \int dz d^2\mathbf{r} |\Psi(z, r)|^2 C_N r^2 \alpha_S(r), \quad (61)$$

which is nearly identical to $\sigma_T(\gamma^* N, x, Q^2)$ of Eq. (17), lacking only $L(r)$ in the integrand. Therefore, this driving term of the triple-pomeron component of the diffraction dissociation of virtual photons satisfies the approximate factorization reminiscent of the factorization properties of the triple-pomeron diagram of conventional Regge theory (Fig. 7a),

$$\frac{M^2 + Q^2}{\sigma_T(\gamma^* N, x, Q^2)} \cdot \left. \frac{d\sigma_D(\gamma^* + N \rightarrow X + N)}{dt dM^2} \right|_{t=0} = A_{3IP}(Q^2) \\ = \frac{\sigma^*(Q^2)}{\sigma_T(\gamma^* N, x, Q^2)} A_{3IP}^*. \quad (62)$$

To the lowest order considered in the perturbation theory, the quantity $A_{3IP}(Q^2)$ does not depend on x . $A_{3IP}(Q^2)$ is the dimensional quantity, and as such it can have had a strong dependence on Q^2 , $A_{3IP}(Q^2) \sim 1/Q^2$ being a plausible guess if $1/\sqrt{Q^2}$ were the only scale relevant to DIS. The fact that $\sigma^*(Q^2)$ and $\sigma_{tot}(\gamma^* N, x, Q^2)$ are nearly identical proves that this is not the case. Furthermore, the right-hand side of Eq. (62) has a very smooth extrapolation down to the real photoproduction limit $Q^2 = 0$, confirming an earlier suggestions^{7,30} that $A_{3IP}(Q^2)$ is close to $A_{3IP}(0)$ as measured in real photoproduction (a more detailed comparison of $A_{3IP}(Q^2)$ with

A_{3IP} for the diffraction dissociation of protons, pions and real photons will be presented elsewhere^{29,42}). For an order-of-magnitude estimate of A_{3IP}^* , in the dominant region of integration in (60) we can take $\mathcal{F}(\mu_G \rho) \sim \exp(-2\mu_G \rho)$, $L(\rho) \sim 1$ and $\sigma(\rho)/\rho^2 \sim C_N \alpha_S(\rho) = 1/2\mu_G$, with the result

$$A_{3IP}^* \sim \frac{27 C_N \alpha_S (4\mu_G^2)^2}{256\pi^2} \frac{\alpha_S (4\mu_G^2)^2}{\mu_G^2} = \frac{\alpha_S (4\mu_G^2)^2}{8\mu_G^2}. \quad (63)$$

With $\mu_G \sim 0.4$ GeV this gives $A_{3IP}^* \sim 0.3$ (GeV)⁻². The experimental data on diffraction dissociation of real photons give $A_{3IP}(0) \approx 0.16$ (GeV)⁻² Ref. 31. This dimensional coupling $A_{3IP}^* \approx A_{3IP}(0)$ emerges as the principal normalization factor of the diffraction dissociation cross section, and Eq. (62) is a starting point of the derivation of the factorization representation (94) to all orders of perturbation theory.

Combining Eq. (62) with the definition Eq. (25), we find the corresponding contribution to the structure function of the pomeron at $x = Q^2/(Q^2 + M^2) \ll 1$,⁷

$$F_2^{(IP)}(x, Q^2) = \frac{4Q^2}{\pi \alpha_{em} \sigma_{tot}(pp)} \sigma^*(x, Q^2) A_{3IP}^* \\ \approx \frac{16\pi A_{3IP}(0)}{\sigma_{tot}(pp)} F_2^{(N)}(x, Q^2) \approx 0.08 F_2^{(N)}(x, Q^2). \quad (64)$$

This describes DIS on the $q\bar{q}$ 'sea' of the pomeron. The relationship (64) shows a deep connection between the triple-pomeron component of the mass spectrum and the sea structure function of the pomeron. Notice the difference between the diffractive excitation of the $q\bar{q}$ state, Fig. 3, and of the $q\bar{q}g$ state, Fig. 7b: in the former the pomeron couples to (anti)quarks and the DIS probes the 'valence' $q\bar{q}$ structure of the pomeron; in the latter the pomeron couples to gluons, and the DIS probes the 'sea' of the pomeron, which can be treated as having been generated from the 'valence' (constituent) gluons of the pomeron.

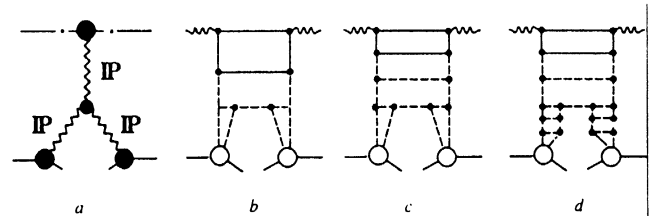


FIG. 7. The triple-pomeron diagrams for the diffraction dissociation of virtual photons in deep inelastic scattering: a) The triple-pomeron diagram, which describes the $\propto 1/M^2$ component of the mass spectrum in the triple-Regge phenomenology of diffraction dissociation. b) The driving term of the triple-pomeron mass spectrum in QCD—the diffraction excitation of the $q\bar{q}g$ Fock state of the photon. c) Diffraction excitation of the many-particle Fock states in the Low-Nussinov approximation for the exchanged pomerons. d) The same as (c) with exchange by the full QCD pomerons.

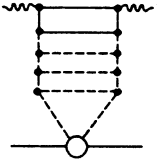


FIG. 8. Gluon-ladder representation of the DLLA pomeron in QCD.

The diffraction dissociation cross section (58) and the pomeron structure function (64) are sensitive to the infra-red regularization, and the normalization of both quantities contains the new dimensional parameter $A_{3\text{IP}}^*$. The important result of the above analysis is that this dimensional parameter $A_{3\text{IP}}^*$ can be inferred approximately from real photoproduction data. Notice a close similarity between Eq. (60) for the normalization of the triple-pomeron mass spectrum and Eq. (21) for the normalization of the mass spectrum for the excitation of the $q\bar{q}$ state. However, whereas Eqs. (60) and (64) predict a flavor-independent relation between the proton and pomeron structure functions, the valence $q\bar{q}$ structure function of the pomeron has a strong flavor dependence.⁷ We now study how these conclusions change when higher-order effects and QCD evolution are included.

4. RISING STRUCTURE FUNCTIONS AND HIGHER-ORDER FOCK STATES OF THE PHOTON. THE BFKL EQUATION

Generalization of the analysis in Sec. 3 to interactions of higher $q\bar{q}g_1\dots g_n$ Fock states of the photon is straightforward. The strong DLLA ordering of gluons

$$x \ll z_n \ll z_{n-1} \ll \dots \ll z_1 \ll z < 1, \quad (65)$$

$$\frac{1}{Q^2} \ll r^2 \ll \rho_1^2 \ll \dots \ll \rho_n^2 \ll R_c^2, \quad (66)$$

is required to have the maximum possible powers of $\log(1/x)$ and $L(Q)$.^{12,26} The quark-loop contributions to the DLLA in the generalized ladder diagrams of Fig. 8 can be neglected. By virtue of the ordering of sizes (66), the $q\bar{q}g_1\dots g_n$ Fock state interacts like the color-singlet octet-octet state, with the inner subsystem $q\bar{q}g_1\dots g_{n-1}$ acting like the pointlike color-octet charge. Henceforth, the generalization of Eq. (51) is

$$\Delta\sigma(r, \rho_1, \dots, \rho_n) = \Sigma(\rho_n) = \frac{3}{2}\sigma(\rho_n). \quad (67)$$

The DLLA wave function is a straightforward generalization of the wave function (50) for the $q\bar{q}g$ Fock state:

$$\begin{aligned} |\Psi(r, \rho_1, \dots, \rho_n)|^2 &= |\Psi(z, r)|^2 \cdot \frac{1}{z_1} \alpha_S(r) \frac{4}{3\pi^2} \frac{r^2}{\rho_1^4} \\ &\times \frac{1}{z_2} \alpha_S(\rho_1) \frac{3}{\pi^2} \frac{\rho_1^2}{\rho_2^4} \cdot \dots \\ &\times \frac{1}{z_n} \frac{3}{\pi^2} \alpha_S(\rho_{n-1}) \frac{\rho_{n-1}^2}{\rho_n^4}. \end{aligned} \quad (68)$$

Notice that the first gluon is radiated by the triplet-antitriplet color-singlet state. The subsequent gluons are radiated by the octet-octet color-singlet state, which brings in the ratio 9/4 of the octet and triplet strong couplings. The corresponding increase in the total cross section equals [here we make explicit use of Eq. (14)]

$$\begin{aligned} \Delta\sigma_{\text{tot}}^{(n)}(\gamma^* N, x, Q^2) &= \frac{4}{3\pi} \cdot \left(\frac{3}{\pi}\right)^{n-1} \int dz d^2\mathbf{r} |\Psi(z, r)|^2 \alpha_S(r) r^2 \cdot \int_r^2 \frac{d\rho_1^2}{\rho_1^2} \alpha_S(\rho_1) \int_{\rho_1^2} \frac{d\rho_2^2}{\rho_2^2} \alpha_S(\rho_2) \dots \int_{\rho_{n-1}^2} \frac{d\rho_n^2}{\rho_n^2} \Sigma(\rho_n) \\ &\times \int_x^z \frac{dz_1}{z_1} \int_x^{z_1} \frac{dz_2}{z_2} \dots \int_x^{z_{n-1}} \frac{dz_n}{z_n} \\ &= \left(\frac{3}{\pi}\right)^n \int dz d^2\mathbf{r} |\Psi(z, r)|^2 \alpha_S(r) C_N r^2 \cdot \int_r^2 \frac{d\rho_1^2}{\rho_1^2} \alpha_S(\rho_1) \int_{\rho_1^2} \frac{d\rho_2^2}{\rho_2^2} \alpha_S(\rho_2) \dots \int_{\rho_{n-1}^2} \frac{d\rho_n^2}{\rho_n^2} \alpha_S(\rho_n) L(\rho_n) \\ &\times \int_x^z \frac{dz_1}{z_1} \int_x^{z_1} \frac{dz_2}{z_2} \dots \int_x^{z_{n-1}} \frac{dz_n}{z_n} \\ &= \int dz d^2\mathbf{r} |\Psi(z, r)|^2 \alpha_S(r) C_N r^2 \left(\frac{12}{\beta_0}\right)^n \frac{1}{(n+1)!} L(r)^{n+1} \frac{1}{n!} \log\left(\frac{z}{x}\right)^n \\ &= \int dz d^2\mathbf{r} |\Psi(z, r)|^2 \sigma(r) \frac{\xi(x/z, r)^n}{(n+1)! n!}. \end{aligned} \quad (69)$$

Therefore, the total photoabsorption cross section can be represented as

$$\sigma_{\text{tot}}(x, Q^2) = \int dz d^2\mathbf{r} |\Psi(z, r)|^2 \sigma\left(\frac{x}{z}, r\right), \quad (70)$$

where

$$\sigma(x, r) = \sigma(r) \sum_{n=0} \frac{\xi(x, r)^n}{(n+1)!n!} \quad (71)$$

is the energy-dependent dipole cross section, which generalizes the Low-Nussinov pomeron to the DLLA pomeron.

The sum in (71) can be evaluated as (we neglect the slowly varying pre-exponential factor)

$$\sum_{n=0} \frac{\xi^n}{(n+1)!n!} = \frac{\partial}{\partial \xi} \sum_{n=1} \frac{\xi^n}{(n!)^2} \propto \exp(2\sqrt{\xi}), \quad (72)$$

leading to

$$\sigma(x, r) \propto \sigma(r) \exp\left[\sqrt{\frac{48}{\beta_0}} \log\left[\frac{1}{\alpha_S(r)}\right] \log\left(\frac{1}{x}\right)\right] \quad (73)$$

and

$$F_2(\text{GLDAP}, x, Q^2) = \frac{Q^2}{4\pi\alpha_{em}} \sigma_{\text{tot}}(x, Q^2) \propto \exp\left[\sqrt{\frac{48}{\beta_0}} \log\left[\frac{1}{\alpha_S(Q^2)}\right] \log\left(\frac{1}{x}\right)\right]. \quad (74)$$

The representation (70) for the photoabsorption cross section in terms of the DLLA dipole cross section (71) is a new result and is presented here for the first time. However, since the perturbative expansion (69) is completely equivalent to the GLDAP evolution equation for the structure function,^{11,12} the result (74) for the DLLA growth of the structure function is identical to the one derived from the GLDAP evolution equations,^{12,41} where it appeared as a rising density $g(\text{GLDAP}, x, Q^2)$ of gluons in the proton. In our light-cone s -channel approach it comes from interactions of the higher $q\bar{q}g_1 \dots g_n$ Fock states of the photon and can be described in terms of the rising DLLA pomeron cross section (71) for the color dipole. As a matter of fact, comparing equations (11) and (28), and making the straightforward generalizations, one can easily show that in the DLLA³⁰

$$\sigma(x, r) = \frac{\pi^2}{3} r^2 \alpha_S(r) x g\left(x, Q^2 \sim \frac{1}{r^2}\right). \quad (75)$$

We note in passing that the cross section (71), (73), (75) obviously does not satisfy the factorization relations usually assumed for the pomeron in standard Regge phenomenology. The QCD evolution analysis of DIS need not assume any factorization of $F_2(x, Q^2)$.

Above, the generalized dipole cross section $\sigma(x, r)$ emerged as the principal quantity that describes diffractive

DIS; see Eq. (70). We are now in a position to write the integral equation directly for the dipole cross section. Specifically, if we expand the dipole cross section as

$$\sigma(x, r) = \sum_{n=0} \frac{1}{n!} \sigma_n(r) \log^n\left(\frac{1}{x}\right), \quad (76)$$

then Eq. (39) is equivalent to

$$\begin{aligned} \sigma_{n+1}(r) = \mathcal{K} \otimes \sigma_n(r) &= \frac{3}{8\pi^3} \int d^2\rho \mu_G^2 \left| g_S(r_1^{(\min)}) K_1(\mu_G \rho) \right. \\ &\times \left. \frac{\rho}{\rho} - g_S(r_2^{(\min)}) K_1(\mu_G R) \frac{R}{R} \right|^2 \\ &\times [\sigma_n(\rho) + \sigma_n(R) - \sigma_n(r)] \end{aligned} \quad (77)$$

and

$$-\frac{\partial \sigma(x, r)}{\partial \log x} = \mathcal{K} \otimes \sigma(x, r). \quad (78)$$

This is our generalization of the BFKL equation for the dipole cross section. In the DLLA studied here, the kernel \mathcal{K} takes a simple form:

$$\sigma_{n+1}(r) = \mathcal{K} \otimes \sigma_n(r) = \frac{3r^2 \alpha_S(r)}{\pi^2} \int_{\rho^2}^{R^2} \frac{d^2\rho}{\rho^4} \sigma_n(\rho). \quad (79)$$

The BFKL scaling limit corresponds to the fixed strong coupling α_S and $\mu_G \rightarrow 0$. By virtue of Eq. (49), in this limit our Eq. (77) takes the form

$$\begin{aligned} \sigma_{n+1}(r) = \mathcal{K} \otimes \sigma_n(r) &= \frac{3\alpha_S}{2\pi^2} \int d^2\rho \frac{r^2}{\rho^2 R^2} \\ &\times [\sigma_n(\rho) + \sigma_n(R) - \sigma_n(r)]. \end{aligned} \quad (80)$$

A proof of the equivalence of this equation to the original BFKL equation and the analysis of solutions of Eq. (77) are presented in Refs. 29 and 42.

5. STRUCTURE FUNCTION OF THE POMERON AND CONSTITUENT GLUONS OF THE POMERON

We now consider diffraction excitation of the higher order $q\bar{q}g_1 \dots g_{n+2}$ Fock states of the photon (Fig. 7c). Large masses M of the excited state

$$M^2 = \frac{m_f^2 + k_q^2}{z_q} + \frac{m_f^2 + k_{\bar{q}}^2}{z_{\bar{q}}} + \sum_{i=1}^{n+2} \frac{k_i^2}{z_i} \quad (81)$$

will be dominated by the softest gluon contribution. The fraction y of the proton's momentum carried off by the pomeron is related to z_{n+2} by [cf. Eq. (40)]

$$z_{n+2} = \frac{x}{y} \quad (82)$$

and

$$\frac{dM^2}{M^2 + Q^2} = \frac{dy}{y} = \frac{dz_{n+2}}{z_{n+2}}. \quad (83)$$

Using the wave function (68), and repeating the consider-

ations that led to Eq. (58), we find the contribution of excitation of the $q\bar{q}g_1 \dots g_{n+2}$ Fock state to the mass spectrum of the diffraction dissociation and to the photon-pomeron cross section:

$$\begin{aligned} \Delta\sigma_{\text{tot}}^{(n+2)}(\gamma^* \text{IP}, Q^2, M^2) &= \frac{16\pi}{\sigma_{\text{tot}}(pp)} (M^2 + Q^2) \frac{d\sigma_D(\gamma^* \rightarrow q\bar{q}g_1 \dots g_{n+2})}{dt dM^2} \Big|_{t=0} \\ &= \frac{1}{\sigma_{\text{tot}}(pp)} \cdot \left(\frac{4}{3\pi}\right) \cdot \left(\frac{3}{\pi}\right)^{n+1} \int dz d^2\mathbf{r} |\Psi(z, \mathbf{r})|^2 \alpha_S(r) r^2 \cdot \int_{\rho^2} \frac{d\rho_1^2}{\rho_1^2} \alpha_S(\rho_1) \dots \int_{\rho_{n-1}^2} \frac{d\rho_n^2}{\rho_n^2} \\ &\quad \times \alpha_S(\rho_n) \int_{\rho_n^2} \frac{d\rho_{n+1}^2}{\rho_{n+1}^2} \alpha_S(\rho_{n+1}) \int_{\rho_{n+1}^2} \frac{d\rho_{n+2}^2}{\rho_{n+2}^2} \Sigma(\rho_{n+2})^2 \mathcal{F}(\mu_G \rho_{n+2}) \\ &\quad \times \int_x^z \frac{dz_1}{z_1} \int_x^{z_1} \frac{dz_2}{z_2} \dots \int_x^{z_n} \frac{dz_{n+1}}{z_{n+1}} \\ &= \frac{1}{\sigma_{\text{tot}}(pp)} \left(\frac{3}{\pi}\right)^n \int dz d^2\mathbf{r} |\Psi(z, \mathbf{r})|^2 \alpha_S(r) r^2 \cdot \int_x^1 \frac{dz_z}{z_1} \dots \int_x^{z_{n-1}} \frac{dz_n}{z_n} \cdot \int_{\rho^2} \frac{d\rho_1^2}{\rho_1^2} \alpha_S(\rho_1) \dots \int_{\rho_{n-1}^2} \frac{d\rho_n^2}{\rho_n^2} \\ &\quad \times \rho_n^2 \alpha_S(\rho_n) \cdot \frac{81}{4\pi^2} \cdot \int_{\rho_n^2} \frac{d\rho_{n+1}^2}{\rho_{n+1}^2} \alpha_S(\rho_{n+1}) \cdot \int_x^{z_n} \frac{dz_{n+1}}{z_{n+1}} \int_{\rho_{n+1}^2} \frac{d\rho_{n+2}^2}{\rho_{n+2}^2} \sigma(\rho_{n+2})^2 \mathcal{F}(\mu_G \rho_{n+2}). \end{aligned} \quad (84)$$

Comparison with Eqs. (11) and (69) shows that the last line of Eq. (84) can be reinterpreted as the dipole cross section for interaction with the pomeron treated as a two-gluon state with the wave function

$$|\Psi_{\text{IP}}(z_g, \mathbf{r})|^2 = \frac{81}{8\pi^4} \cdot \frac{1}{z_g} \cdot \frac{1}{\sigma_{\text{tot}}(pp)} \left[\frac{\sigma(r)}{r^2}\right]^2 \mathcal{F}(\mu_G r), \quad (85)$$

where

$$z_g = \frac{z_{n+2}}{z_{n+1}} \quad (86)$$

is the fraction of pomeron's momentum carried by the gluon.

Indeed, making use of Eq. (43) for the vertex function of the two-body system, the dipole cross section $\sigma_{2g}(\rho)$ for the scattering on the gluon-gluon state can be written as

$$\begin{aligned} \sigma_{2g}(\rho) &= 2\pi\rho^2 \alpha_S(\rho) \int dz_g \int d^2\mathbf{r} |\Psi_{2g}(z, \mathbf{r})|^2 \\ &\quad \times \int_0^{1/\rho^2} \frac{dk^2 k^2}{(k^2 + \mu_G^2)^2} \alpha_S(k^2) [1 - \exp(i\mathbf{k}\mathbf{r})]. \end{aligned} \quad (87)$$

The factor 3/2 difference from Eqs. (11) and (14) is due to the ratio 9/4 of the gluon (octet) and the quark (triplet) strong couplings and the ratio 2/3 of the number of

constituent gluons in the pomeron and the number of constituent quarks in the proton. A series of transformations of the integrand of (87),

$$\begin{aligned} \sigma_{2g}(\rho) &= 2\pi\rho^2 \alpha_S(\rho) \int dz_g \int d^2\mathbf{r} |\Psi_{2g}(z_g, \mathbf{r})|^2 \\ &\quad \times \int_{1/\rho^2}^{1/\rho^2} \frac{dk^2}{k^2} \alpha_S(k^2) \\ &= 2\pi\rho^2 \alpha_S(\rho) \int dz_g \int d^2\mathbf{r} |\Psi_{2g}(z_g, \mathbf{r})|^2 \\ &\quad \times \int_{\rho^2} \frac{d\rho_1^2}{\rho_1^2} \alpha_S(\rho_1) \\ &= 2\pi\rho^2 \alpha_S(\rho) \int_{\rho^2} \frac{d\rho_1^2}{\rho_1^2} \alpha_S(\rho_1) \\ &\quad \times \int dz_g \int_{\rho_1^2} d^2\mathbf{r} |\Psi_{2g}(z_g, \mathbf{r})|^2, \end{aligned} \quad (88)$$

and comparison with the last line of Eq. (84) complete the derivation of the wave function (85). This is one of the central results of the present paper.

The wave function $\Psi_{2g}(z_g, \mathbf{r})$ gives the distribution of the 'valence' gluons $g_{\text{IP}}(z_g)$ in the pomeron

$$g_{\text{IP}}(z_g) = \int d^2\mathbf{r} |\Psi_{2g}(z_g, \mathbf{r})|^2. \quad (89)$$

The perturbative expansion (84) describes the QCD evolution of this 'valence' gluon distribution. The above derivation holds at $z_g \ll 1$; the neighborhood $z_g \sim 1$ requires special consideration. Only $z_g \sim 1$ is important in the DLLA. The radius of the pomeron $R_P \sim R_N$, $1/\mu_G$, and it is controlled by both the form factor $\mathcal{F}(\mu_{GP})$ and the behavior of $\sigma(r)$ in the saturation regime. The absolute normalization of the flux of soft gluons in the pomeron is given by the familiar coupling A_{3IP}^* :

$$\begin{aligned} z_g g_{IP}(z_g) &= \frac{81}{8\pi^3} \cdot \frac{1}{\sigma_{\text{tot}}(pp)} \int dr^2 \left[\frac{\sigma(r)}{r^2} \right]^2 \mathcal{F}(\mu_{GP}) \\ &= \frac{128\pi}{9} \cdot \frac{A_{3IP}^*}{\sigma_{\text{tot}}(pp)} \sim 0.06. \end{aligned} \quad (90)$$

Extrapolation of (90) to large z_g as well yields an estimate of the gluon momentum integral for the pomeron,

$$\langle x_g \rangle_{IP} = \int_0^1 dx x g_{IP}(x) \approx \frac{128\pi}{9} \cdot \frac{A_{3IP}^*}{\sigma_{\text{tot}}(pp)} \sim 0.06. \quad (91)$$

The momentum integral for the 'valence' (anti)quarks of the pomeron, discussed in Section 2.4, was estimated in Ref. 7 with the result $\langle x_v(q\bar{q}) \rangle_P \sim 0.1$. Equation (64) gives a few per cent estimate for the momentum integral for the sea (anti)quarks. Here we merely emphasize that the pomeron need not be regarded as a particle, and on purely theoretical grounds there is no reason why the momentum integral for gluons and (anti)quarks in the pomeron must add to 100%.⁷

Henceforth, we identify three components of the input for the QCD evolution of the pomeron structure function: i) the valence quark-antiquark component with the structure function (25) (see Ref. 7; for a detailed analysis); ii) the valence gluon distribution with the structure function (90); iii) the sea (anti)quark distribution given by Eq. (64). All these input parton distributions are sensitive to the infrared regularization. There is nothing wrong with this sensitivity: the infrared sensitivity of the parton distributions is inherent to the QCD-improved parton model. In the conventional parton model phenomenology it is hidden in the parametrization of the parton densities at small factorization scale, which is then used as an input in the QCD evolution analysis of the scaling violations. The important finding is that the absolute normalization of the sea and gluon distributions in the pomeron is determined by one and the same flavor-independent dimensional constant A_{3IP}^* , which must be approximately equal to the triple-pomeron coupling as measured in real photoproduction. The normalization of the valence $q\bar{q}$ structure function of the pomeron is given by a very similar but flavor-dependent dimensional constant [cf. equations (21), (58) and (60)]. In the above DLLA analysis we omitted the quark loops in the ladder diagrams for the pomerons. These quark loops will automatically be included in the GLDAP-evolution calculation of the structure function of the pomeron starting with the aforementioned input parton distributions in the pomeron.

6. FLUX OF QCD POMERONS IN THE PROTON

To complete our analysis we must replace the Low-Nussinov two-gluon pomeron in the lower part of the diagrams in Fig. 7c by the full QCD pomeron—the sum of the triple-ladder diagrams of Fig. 7d. This is done by replacing the dipole cross section $\sigma(\rho)$ by $\sigma(y, \rho)$ in the last line of Eq. (84), where y is the fraction of the proton's momentum carried by the pomeron. The diffraction dissociation cross section thus calculated will differ from that of Sec. 5 only by the y -dependent factor

$$f_{IP}(y) = \frac{\int d\rho^2 [\sigma(y, \rho)/\rho^2]^2 \mathcal{F}(\mu_{GP})}{\int d\rho^2 [\sigma(\rho)/\rho^2]^2 \mathcal{F}(\mu_{GP})}. \quad (92)$$

What is the proper interpretation of $f_P(y)$?

We would like to preserve the most important result of the above analysis—the representation of the diffraction dissociation cross section through the GLDAP-evolving structure function of the pomeron. The scaling variable of the photon-pomeron scattering (3) equals $x_P = Q^2/(Q^2 + M^2) = x/y$, so that

$$\frac{dM^2}{M^2 + Q^2} = \frac{dy}{y}. \quad (93)$$

With allowance for the factor $f_P(y)$, Eq. (92) for the diffraction dissociation cross section can be written in the factorized form

$$\left. \frac{d\sigma_D}{dt dy} \right|_{t=0} = \frac{\sigma_{\text{tot}}(pp)}{16\pi} \cdot \frac{4\pi\alpha_{em} f_{IP}(y)}{Q^2} \frac{1}{y} F_2^{(IP)}\left(\frac{x}{y}, Q^2\right), \quad (94)$$

which has the conventional parton model representation, with $f_P(y)/y$ being the flux of pomerons treated as partons of the proton. In order not to introduce any spurious dependence on the kinematic variables x and y , the coefficient $\sigma_{\text{tot}}(pp)/16\pi$ in (94) must be assumed constant, for instance fixing $\sigma_{\text{tot}}(pp) = 40$ mb. Because the pomeron is not the particle with the well-defined couplings (residues) and spin, and because in QCD the pomeron does not factorize, the Regge theory convention (1) is not unique. The coefficient $\sigma_{\text{tot}}(pp)/16\pi$ is the convention-dependent normalization constant for the correct dimensionality of the diffraction dissociation cross section in terms of the dimensionless structure function or vice versa. The absolute normalizations of the flux of pomerons and of the pomeron structure function are the convention-dependent ones: it is always the product of the two quantities that enters the experimentally observable cross sections. Equation (94) shows how QCD evolution effects and the rising dipole cross section $\sigma(x, \rho)$ modify the $1/M^2$ law (4) for the mass spectrum in the triple-pomeron region. The factorization (94) bears a certain resemblance to the usual Regge theory factorization in the triple-Regge region. We emphasize that we have derived (94) neither assuming nor using any of the Regge theory factorization relations.

The three pomerons in the triple-pomeron diagram are described by different QCD ladder diagrams. The top pomeron of Fig. 7d is in the LLA regime: the relevant sizes vary along the ladder from $\rho_{n+2}^2 \sim R_{IP}^2$ in the bottom cell of

the ladder down to $r^2 \sim 1/Q^2$ in the top, quark-antiquark, cell of the ladder. For this reason we can introduce the structure function of the pomeron. By contrast, the exchanged pomerons in the lower part of Fig. 7d are the soft pomerons: since $\rho_{n+2}^2 \sim R_{IP}^2 \sim R_N^2$, the situation is reminiscent of the pomeron contribution to the typical hadronic cross section; see Eq. (16). The predictive power of QCD for the hadronic total cross section is still very limited.^{17,19,29,43} The empirical observation is that the hadronic cross sections and the real photoabsorption cross section¹⁴ have a very weak dependence on energy $\nu \sim m_N/x$, much weaker than the steep rise in the DIS structure functions with $1/x$. The dipole cross section (71) is consistent with this property: it is essentially flat vs $1/x$ at large, hadronic, size r , and the smaller the size r , the steeper the rise in $\sigma(x,r)$ with $1/x$.

This rise has a definite impact on the radius of the pomeron. Namely, the replacement of $\sigma(r)$ by $\sigma(x,r)$ leads to the effective wave function of the pomeron

$$|\Psi_{IP}(y, z_G, r)|^2 = \frac{81}{8\pi^4} \cdot \frac{1}{z_G} \times \frac{1}{\sigma_{\text{tot}}(pp)} \left[\frac{\sigma(y, r)}{r^2} \right]^2 \mathcal{F}(\mu_G r). \quad (95)$$

With the rising generalized dipole cross section $\sigma(y, r)$, the ratio $\sigma(y, r)/r^2$ will rise toward small r , so that the effective radius of the pomeron $R_p(y)$ will decrease as $y \rightarrow 0$. The GLDAP evolution equations hold at $R_i^2 Q^2 \gg 1$, where the R_i are the relevant hadronic radii. If one would like to formulate the input for the GLDAP evolution at a certain fixed Q_0^2 , then because of the decreasing radius of the pomeron, the GLDAP applicability condition will be violated at very small values of $y \lesssim y_c(Q_0^2)$ such that

$$R_{IP}(y_c(Q_0^2))^2 Q_0^2 = 1. \quad (96)$$

The factorization of the diffraction dissociation cross section into the flux of pomerons and the structure function of pomerons Eq. (94) will break down at $y < y_c(Q_0^2)$. Our criterion (96) for the breakdown of GLDAP evolution is different from the GLR criterion¹⁹ (for a review and references, see Ref. 22).

7. UNITARIZATION OF THE RISING STRUCTURE FUNCTIONS

7.1. Rising cross sections and s-channel unitarity.

The rising cross section $\sigma(x, r)$ Eq. (71) conflicts with the s-channel unitarity at sufficiently large $1/x$. The s-channel unitarity constraint is best formulated in the impact parameter representation (the partial wave expansion) and reads

$$\Gamma(b) < 1. \quad (97)$$

The profile function $\Gamma(b)$ is related to the elastic scattering amplitude $f(\vec{q})$ such that

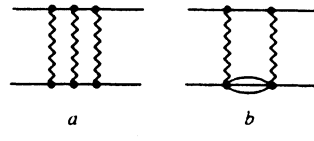


FIG. 9. s channel iteration of the pomeron exchange: a) In the approximation of elastic intermediate states. b) Contribution of the inelastic intermediate states (diffraction dissociation of the target) to the s-channel iteration of the pomeron exchange.

$$f(q) = 2i \int d^2b \Gamma(b) \exp(-iqb) = i\sigma_{\text{tot}} \exp\left(-\frac{1}{2} B_{el} q^2\right). \quad (98)$$

Here B_{el} is the diffraction slope of the elastic scattering. The Gaussian parametrization (98) is viable for the purposes of the present discussion⁴⁵ and gives

$$\Gamma(b) = \frac{\sigma_{\text{tot}}}{4\pi B_{el}} \exp\left(-\frac{b^2}{2B_{el}}\right). \quad (99)$$

The profile function of the bare pomeron exchange $\Gamma_0(b)$ defined for the rising cross section (71) will overshoot the s-channel unitarity bound at sufficiently small x .

There is no unique prescription as to how to impose the s-channel unitarity constraint on the rising cross sections. The most used procedures are the eikonal^{46,47}

$$\Gamma(b) = 1 - \exp[-\Gamma_0(b)] = \sum_{\nu=1}^{\infty} \frac{(-1)^{\nu-1}}{\nu!} \Gamma_0(b)^\nu \quad (100)$$

and the \mathcal{K} -matrix^{43,48}

$$\Gamma(b) = \frac{1}{1 + \Gamma_0(b)} = \sum_{\nu=1}^{\infty} (-1)^{\nu-1} \Gamma_0(b)^\nu \quad (101)$$

s-channel unitarizations. Both produce $\Gamma(b)$ which satisfies the unitarity bound (97). To leading order in the s-channel unitarization, the unitarized profile function reads

$$\Gamma(b) \approx \Gamma_0(b) - \frac{1}{2} \chi \Gamma_0(b)^2, \quad (102)$$

with $\chi=1$ for the eikonal unitarization, and $\chi=2$ for the \mathcal{K} -matrix unitarization. The eikonal unitarization is routinely used in high-energy physics⁴⁹ and sums the s-channel iterations of the bare pomeron exchange (Fig. 9a) when only elastic scattering intermediate states are included in the s-channel. Besides the elastic scattering states as in Fig. 9a, one must include the inelastic intermediate states of Fig. 9b, which correspond to the diffraction dissociation of the target nucleon. These inelastic intermediate states lead to an enhancement of the double and higher-order rescattering terms in expansions (100,101).^{47,50,51} If one starts with the eikonal unitarization (which is an assumption), and includes the corrections for the diffraction dissociation of the target nucleons, then⁵¹

$$\chi \approx 1 + \frac{\sigma_D(p \rightarrow X)}{\sigma_{el}(pp)} \sim 1.5. \quad (103)$$

In fact, the \mathcal{N} -matrix prescription (101) was obtained in Ref. 45 starting with the eikonal unitarization of πN scattering and including the inelastic intermediate states in the QCD-inspired model of the diffraction dissociation of pions.

7.2. Shadowing correction to the proton structure function.

We now discuss unitarization (shadowing, absorption) effects in DIS, taking full advantage of the diagonalization of the S -matrix in the (ρ, z) -representation, which enables us to impose s -channel unitarization on all multiparton cross sections $\sigma_n(\mathbf{r}, \rho_1, \dots, \rho_n)$ at all values of \mathbf{r} and ρ_i . Although there is no unique s -channel unitarization procedure, we can still develop a sound phenomenology. We identify the cross section (71), which leads to the GLDAP-evolving structure function $F_2^{(N)}$ (GLDAP, x, Q^2), with bare-pomeron exchange. The bare-pomeron structure function $F_2^{(N)}$ (GLDAP, x, Q^2) is a linear functional of the density of partons in the proton:

$$\begin{aligned} F_2^{(p)}(\text{GLDAP}, x, Q^2) &= \frac{Q^2}{4\pi\alpha_{em}} \sigma_{\text{tot}}(\text{GLDAP}, x, Q^2) \\ &= \sum_i e_i^2 x [q_i(\text{GLDAP}, x, Q^2) \\ &\quad + \bar{q}_i(\text{GLDAP}, x, Q^2)]. \quad (104) \end{aligned}$$

The construction of the unitarized photoabsorption cross section goes as follows. For each Fock state we define the bare $\Gamma_0(b)$ and the unitarized $\Gamma(b)$ profile functions and the bare σ_0 and the unitarized cross section $\sigma^{(U)}$:

$$\begin{aligned} \sigma^{(U)} &= 2 \int d^2\vec{b} \Gamma(b) \\ &= 2 \int d^2\vec{b} \Gamma_0(b) - 2 \int d^2\vec{b} [\Gamma_0(b) - \Gamma(b)] \\ &= \sigma_0 - \Delta\sigma^{(sh)}. \quad (105) \end{aligned}$$

Let us derive the shadowing (unitarity) correction to the scattering of the $q\bar{q}$ Fock state of the photon. To leading order in $\Gamma_0(b)$, Eqs. (102) and (99) give

$$\Delta\sigma^{(sh)}(\rho) \approx \chi \frac{\sigma(\rho)^2}{16\pi B(\rho)}, \quad (106)$$

and the shadowing correction to the total photoabsorption cross section equals

$$\begin{aligned} \Delta\sigma_{\text{tot}}^{(sh)}(\gamma^* N, x, Q^2) &= \int dz d^2\rho |\Psi(z, \rho)|^2 \Delta\sigma^{(sh)}(\rho) \\ &\approx \chi \int dz d^2\rho |\Psi(z, \rho)|^2 \frac{\sigma(\rho)^2}{16\pi B(\rho)} \end{aligned}$$

$$\begin{aligned} &= \chi \int dM^2 \int dt \frac{d\sigma_D(\gamma^* \rightarrow q + \bar{q})}{dt dM^2} \\ &= \chi \int dM^2 \frac{1}{B_D(M^2)} \frac{d\sigma_D(\gamma^* \rightarrow q + \bar{q})}{dt dM^2} \Big|_{t=0} \\ &= \chi \int \frac{dM^2}{M^2 + Q^2} \frac{\sigma_{\text{tot}}(pp)}{16\pi B_D(M^2)} \\ &\quad \times \sigma_{\text{tot}}(\gamma^* \text{IP} \rightarrow q + \bar{q}, M^2). \quad (107) \end{aligned}$$

Here $B_D(M^2)$ is the diffraction slope for the diffraction excitation of the mass M . The shadowing correction to the total photoabsorption cross section equals the diffraction dissociation cross section times the enhancement parameter $\chi \approx (1-2)$. The generalization of Eq. (107) to interactions of the higher Fock states of the photon is straightforward. Making use of Eq. (94), we obtain the shadowing correction to the structure function of the proton

$$\begin{aligned} \Delta F_2^{(sh)}(x, Q^2) &= \chi \frac{\sigma_{\text{tot}}(pp)}{16\pi B_{3\text{IP}}} \int_x^{y_m} \frac{dy}{y} f_{\text{IP}}(y) F_2^{(\text{IP})} \\ &\quad \times \left(\frac{x}{y}, Q^2 \right) \frac{B_{3\text{IP}}}{B_D(M^2)}. \quad (108) \end{aligned}$$

(The slope $B_{3\text{IP}}$ and the end-point y_m of the pomeron distribution will be defined below.) Ignore for the moment the mass dependence of the slope $B_D(M^2)$. Since $F_2^{\text{IP}}(x, Q^2)$ satisfies the GLDAP evolution, the convolution representation (108) implies that the shadowing correction to the proton structure function also satisfies the GLDAP evolution equations! Experimentally, in all hadronic reactions and in the diffraction dissociation of real photons, the slope $B_D(M^2)$ exhibits a similar dependence on the excited mass M :³¹ in the triple-pomeron region the slope is constant to a good approximation,

$$B_D(M^2) = B_{3\text{IP}} \approx \frac{1}{2} B_{el}(hN), \quad (109)$$

whereas in the resonance excitation region,

$$B_D(M^2) \sim B_{el}(hN). \quad (110)$$

In the DIS the counterpart of excitation of resonances is the excitation of the $q\bar{q}$ Fock states of the photon, for which we expect the slope (110), whereas for the higher Fock states and heavier masses the slope (109) is more appropriate. These assumptions can be tested at HERA. Consequently, as compared with the pomeron structure function measured in diffraction dissociation, in the shadowing structure function (108) the 'valence' $q\bar{q}$ component of the pomeron enters with the suppression factor $B_{3\text{IP}}/B_D(M^2) \approx 1/2$, which does not affect the QCD evolution properties. We conclude that the unitarized structure function of DIS,

$$F_2^{(N)}(x, Q^2) = F_2^{(N)}(\text{GLDAP}, x, Q^2) - \Delta F_2^{(sh)}(x, Q^2), \quad (111)$$

satisfies the linear GLDAP evolution equation.

7.3. Brief phenomenology of the shadowing correction to the proton structure function.

According to Eq. (107), the relative shadowing correction to the proton structure function equals the fraction w_{DD} of DIS which goes via diffraction dissociation of photons times the enhancement parameter χ . In diffraction dissociation events, the proton changes its longitudinal momentum p_L slightly, $\Delta p_L/p_L = y < y_m \lesssim 0.1$, and appears in the final state separated from the hadronic debris of the photon by the rapidity gap

$$\Delta\eta = \log\left(\frac{1}{y}\right). \quad (112)$$

The standard definition of the diffraction dissociation corresponds to $\Delta\eta \gtrsim \Delta\eta_{\min} = 2 - 2.5$. The maximal kinematically allowed value of the rapidity gap is $\eta_{\max} = \log(1/x)$. The estimate of w_{DD} is particularly easy when the pomeron and proton structure functions are approximately constant. In this case $f_p(y) = 1$, the rapidity gap distribution is flat, which is a signature of the triple-pomeron mechanism,¹ and combining equations (64) and (107) we find⁷

$$\begin{aligned} w_{DD}(x) &\approx \frac{A_{3\text{IP}}(0)}{B_{3\text{IP}}} \int_x^{y_m} \frac{dy}{y} \\ &= \frac{A_{3\text{IP}}(0)}{B_{3\text{IP}}} \int_{\Delta\eta_{\min}}^{\eta_{\max}} d\Delta\eta \\ &= \frac{A_{3\text{IP}}(0)}{B_{3\text{IP}}} \log\left(\frac{y_m}{x}\right), \end{aligned} \quad (113)$$

which is roughly Q^2 -independent. Numerically, $A_{3\text{IP}}(0)/B_{3\text{IP}} \approx 0.03$, and in Ref. 7 we gave an estimate $w_{DD} \approx 0.15$ at $x \sim 10^{-3}$ and $Q^2 \sim 30$ (GeV/c)². This prediction is consistent with the first determinations of w_{DD} by the ZEUS collaboration at HERA.³²

For a somewhat more realistic evaluation of w_{DD} , let us assume that

$$f_{\text{IP}}(y) \sim \left(\frac{y_m}{y}\right)^{2\Delta}, \quad (114)$$

where $\Delta = \alpha_{\text{IP}}(0) - 1 \sim 0.1$, as suggested by the pomeron phenomenology of the hadronic cross sections.^{16,17} We also assume that at small x the structure functions rise as $(1/x)^\delta$ with the same exponent δ for the proton and pomeron. The analysis of Ref. 33 gives $\delta(Q^2) \sim 0.21$ at $Q^2 = 4$ (GeV/c)² and $\delta(Q^2) \sim 0.31$ at $Q^2 = 15$ (GeV/c)². Experience with the QCD evolution analysis suggests that the ratio $F_2^{(\text{IP})}(x, Q^2)/F_2^{(N)}(x, Q^2)$ will vary only weakly with Q^2 , so that Eq. (64) can be used for the relative normalization of the proton and pomeron structure functions. Then,

$$\begin{aligned} w_{DD}(x) &\approx \frac{A_{3\text{IP}}(0)}{B_{3\text{IP}}} \int_{\Delta\eta_{\min}}^{\eta_{\max}} d\Delta\eta \exp[-\gamma(\Delta\eta - \Delta\eta_{\min})] \\ &= \frac{A_{3\text{IP}}(0)}{B_{3\text{IP}}} \cdot \frac{1}{\gamma} \left[1 - \left(\frac{x}{y_m}\right)^\gamma \right], \end{aligned} \quad (115)$$

and to the extent that $\gamma = \delta - 2\Delta \ll 1$, and

$\gamma(\eta_{\max} - \Delta\eta_{\min}) \lesssim 1$, we have still an approximately flat rapidity gap distribution, and again obtain the estimate (113) for w_{DD} . Consequently, we predict a rather large shadowing effect in the proton structure function

$$\frac{\Delta F_2^{(sh)}(x, Q^2)}{F_2^{(p)}(x, Q^2)} \approx \chi w_{DD}(x), \quad (116)$$

which persists at all Q^2 . In the kinematic range of the DIS at HERA, the shadowing effect can be as large as $\sim 30\%$. A more detailed phenomenology of the shadowing corrections is presented in Ref. 33.

7.4. Unitarization and shadowing correction to the parton densities.

Since $F_2^{(sh)}(x, Q^2)$ satisfies the linear GLDAP evolution, the shadowing correction to the proton structure function can be reabsorbed into the modification of parton densities in the proton. For instance, the shadowed density of gluons in the proton will equal

$$\begin{aligned} g(x, Q_0^2) &= g(\text{GLDAP}, x, Q_0^2) \\ &\quad - \chi \frac{\sigma_{\text{tot}}(pp)}{16\pi B_{3\text{IP}}} \int_x^{y_m} \frac{dy}{y^2} f_{\text{IP}}(y) g_{\text{IP}}\left(\frac{x}{y}\right). \end{aligned} \quad (117)$$

Similarly, the valence and sea $q\bar{q}$ distributions in the pomeron will modify the sea quark distribution in the proton. Here we merely note that whereas the GLDAP-defined parton distributions satisfy the momentum sum rule

$$\begin{aligned} \sum_{p=q, \bar{q}, g} \langle x_p \rangle &= \int_0^1 dx x \left\{ g(\text{GLDAP}, x, Q^2) \right. \\ &\quad + \sum_i [q_i(\text{GLDAP}, x, Q^2) \\ &\quad \left. + \bar{q}_i(\text{GLDAP}, x, Q^2)] \right\} = 1, \end{aligned} \quad (118)$$

because of the shadowing correction this sum rule does not hold for the experimentally measured shadowed (unitarized) parton distributions. A crude estimate of violation of the momentum sum rule (118) is

$$\Delta\Sigma_x = 1 - \sum_{p=q, \bar{q}, g} \langle x_p \rangle \sim y_m \cdot \frac{A_{3\text{IP}}^*}{B_{3\text{IP}}} \sim 0.003. \quad (119)$$

With the $\approx 2\%$ systematic normalization errors in the most accurate measurements of $F_2^{(N)}(x, Q^2)$, presently the momentum sum rule can not be tested to better than 5%.⁵² The concept of the fusion (recombination) of partons must be used with much caution. For instance, the shadowing correction to the density of gluons Eq. (118) is not proportional to $g(x, Q^2)^2$ as often stated in the literature (see Refs. 19–22 and Sec. 7.6 below). Indeed, the shadowing term is proportional to $A_{3\text{IP}}^*$, the integrand of which is

$$\propto [\sigma(y, r)/r^2]^2 \propto [xg(x, Q_{\text{IP}}^2 = 1/r^2)]^2$$

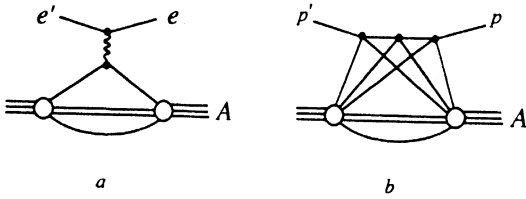


FIG. 10. The archetype operator product expansion: a) Impulse approximation diagram for electron–nucleus scattering, which is a linear probe of the nuclear charge distribution. b) Multiple scattering diagrams which unitarize the proton–nucleus elastic scattering amplitude.

and the integration is dominated by large hadronic values of $r \sim R_P$ and small virtualities of the fusing gluons $Q_{IP}^2 \sim 1/R_{IP}^2$ ^{23,24,36}

Because of shadowing, the parton distributions inferred from the GLDAP evolution analysis of the DIS structure functions will be different from the operator-product expansion (OPE) defined parton distributions, which define the impulse approximation component $F_2^{(N)}$ (GLDAP, x, Q^2) in Eq. (104). To this end, an analogy with the comparison between electron–nucleus and proton–nucleus scattering is instructive: the elastic eA scattering is described by the sum of the impulse approximation diagrams of Fig. 10a and is a linear functional of the nuclear charge density. The eA scattering amplitude measures the charge of the nucleus, which equals the sum of charges of its constituents (nucleons). Choosing an appropriate external field, one can study the whole sequence of the nuclear matrix elements that will be sensitive to the momentum distribution of nucleons in the nucleus. For instance, considering the scattering of the nucleus in the center-of-mass frame, one can derive the momentum sum rule that the constituent nucleons carry the total momentum of the nucleus. ³⁶ Under the strong condition that scattering in external fields is described by the impulse approximation, i.e., by the exchange of the single quantum of the external field, having measured the scattering amplitudes in a variety of external fields one can reconstruct the momentum distribution of nucleons in the nucleus. One would recognize in the above the standard OPE definition of the parton densities (for instance, see the textbooks listed as Ref. 53). In pA elastic scattering, the impulse approximation amplitude $f_A(\vec{q}) = Af_N(\vec{q})G_A(\vec{q})$, where $G_A(\vec{q})$ is the body form factor of the nucleus, has the profile function $\Gamma_A(b) \sim A^{1/3}$, which grossly overshoots the unitarity bound (97). Consequently, the pA scattering amplitude is subject to large unitarization corrections (Fig. 10b) and is a nonlinear functional of the nuclear matter density.

In this context, the GLDAP approach corresponds to the impulse approximation and Eq. (104) gives the *linear* relationship between the Compton scattering amplitude and the parton densities. The shadowing term is an apparently *nonlinear* functional of the density of partons in the proton, but we have proven that this nonlinearity can be cast in the form of the renormalization of the parton densities, with retention of the linear GLDAP evolution properties.

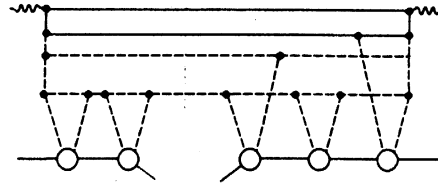


FIG. 11. Absorption (unitarization) corrections to the diffraction excitation of the $q\bar{q}g_1 \dots g_n$ Fock state of the photon. The vertical dashed line shows the unitarity cut.

7.5. Higher-order unitarity corrections and fusion of partons.

Higher-order unitarity corrections, i.e., multiple-pomeron exchanges Figs. 1b, 1d, 9, do technically give rise to photon–multipomeron interactions, which casts doubt on the very definition of the photon–pomeron cross section and pomeron structure function, Eqs. (1) and (2). The remarkable observation is that one can still describe the diffraction dissociation cross section in terms of the pomeron structure function and the factorization representation Eq. (94), and these $\gamma^*(nIP)$ interactions only slightly modify $f_{IP}(y)$ and the simple relationship (108) between the shadowing structure function and the pomeron structure function.

Let us start with the unitarization of the diffraction dissociation cross section. The s -channel iterations of the QCD pomeron exchange to the left and to the right of the unitarity cut in Fig. 11 separately sum to the unitarized dipole cross section. For the $q\bar{q}$ Fock state one must unitarize $\sigma(y, r) = \frac{2}{3}\sigma(y, r)$. Barring the $q\bar{q}$ state, the flux of pomerons $f_{IP}^{(D)}(y)$ which enters the diffraction dissociation cross section must be calculated with the substitution

$$\sigma(y, r)^2 \rightarrow \left(\frac{4}{9}\right)^2 \Sigma^{(U)}(y, r)^2 \quad (120)$$

in the pomeron wave function (95), so that

$$f_{IP}^{(D)}(y) = \left(\frac{4}{9}\right)^2 \cdot \frac{\int d^2r [\Sigma^{(U)}(y, r)/r^2]^2 \mathcal{F}(\mu_G r)}{\int d^2r [\sigma(r)/r^2]^2 \mathcal{F}(\mu_G r)}. \quad (121)$$

Apart from this minor change, the perturbative QCD expansion (84) will retain its form.

Similarly, in the case of the shadowing correction, Fig. 12, the higher-order unitarity corrections are accounted for by the substitution

$$\begin{aligned} \sigma(y, r)^2 &\rightarrow \frac{16\pi B_{3IP}}{\chi} \cdot \left(\frac{4}{9}\right)^2 \cdot \Delta \Sigma^{(sh)}(y, r) \\ &= \frac{16\pi B_{3IP}}{\chi} \cdot \left(\frac{4}{9}\right)^2 \cdot [\Sigma(y, r) - \Sigma^{(U)}(y, r)], \end{aligned} \quad (122)$$

so that $\chi f_{IP}(y)$ in Eq. (108) will be replaced by

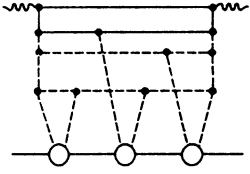


FIG. 12. Unitarization of the scattering amplitude for the $q\bar{q}g_1 \dots g_n$ Fock state of the photon by the s -channel iteration of the QCD pomeron exchange.

$$\chi f_{\text{IP}}^{(sh)}(y) = 16\pi B_{3\text{IP}} \cdot \left(\frac{4}{9}\right)^2 \times \frac{\int dr^2 \{ [\Sigma(y,r) - \Sigma^{(U)}(y,r)] / r^4 \} \mathcal{F}(\mu_G r)}{\int dr^2 [\sigma(r) / \rho^2]^2 \mathcal{F}(\mu_G \rho)}. \quad (123)$$

Again, for the $q\bar{q}$ state one must unitarize $\sigma(y,r)$. The higher-order unitarity corrections make the fluxes $f_{\text{IP}}^{(D)} \times (y)$ for the diffraction dissociation and $f_{\text{IP}}^{(sh)}(y)$ for the shadowing correction slightly different, both in absolute normalization and in y -dependence.

Equations (121) and (123) sum in a very compact form all multiple pomeron exchanges in the s channel (Figs. 11 and 12). The origin of this remarkable result is simple: the interaction cross section of the n -parton Fock state of the photon is dominated by the spatial extent of the softest gluon that acts as a constituent gluon of the pomeron. This corresponds to dominance of the multipomeron exchange diagrams of Fig. 13. Consequently, the unitarization affects only the normalization of the pomeron wave function, and not the QCD evolution properties of the pomeron structure function.

The shadowing structure function can be reinterpreted in terms of the fusion of partons from the overlapping pomerons emitted by the same nucleon, which reduces the total density of partons. The fusion of partons from different nucleons of the nucleus was first introduced in 1975,⁵⁴ and remains a viable mechanism for the nuclear shadowing in DIS.^{23,24,36} However, this interpretation must be taken with the grain of salt. The bare GLDAP cross section (75) is a linear functional of the density of gluons, and the unitarized cross sections $\sigma^{(U)}(x,r)$, $\Sigma^{(U)}(x,r)$ contain the

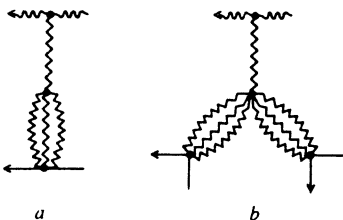


FIG. 13. The dominant multipomeron interactions in deep inelastic scattering.

terms $\propto (-1)^{n+1} [xg(x,r)]^n$, which are sign-alternating and defy the naive probabilistic interpretation. In more general terms, the multigluon exchange contribution is proportional to the many-gluon density matrix, the elements of which are not necessarily positive-definite. Evidently, this quantum-mechanical property is missed in the probabilistic approach to fusion.

7.6. Unitarization and linear GLDAP versus nonlinear GLR evolution equations.

There was much discussion of the unitarization of rising structure functions in the framework of the so-called Gribov–Levin–Ryskin (GLR) nonlinear evolution equation (see Ref. 19; for a recent review with many references, see Ref. 22). Here we briefly comment on the origin of the nonlinear term in the GLR equation, following the standard derivation of the evolution equations.^{11–13} (We are only interested in $x \ll 1$.) One starts by evaluating the derivative¹²

$$Q^2 \frac{\partial}{\partial Q^2} F_2(x, Q^2) \propto Q^2 \frac{\partial}{\partial Q^2} [Q^2 \sigma_{\text{tot}}(\gamma^* N, x, Q^2)]. \quad (124)$$

In Sec. 2, we decomposed $Q^2 \sigma_{\text{tot}}(\gamma^* N, x, Q^2)$ into a non-LLA component (18), which we can neglect, and an LLA component (17), in which all the explicit dependence on Q^2 is concentrated in the integration limit. This is the crucial point, since taking the derivative (124) and making use of Eq. (75), one obtains one of the small- x GLDAP equations

$$Q^2 \frac{\partial}{\partial Q^2} [xq(x, Q^2)] \propto Q^2 \sigma(1/Q) \propto x \alpha_S(Q^2) g(x, Q^2), \quad (125)$$

in which both the right- and left-hand sides are evaluated at the same value of Q^2 . Note that this property is a result of the singular behavior of the integrand in Eq. (17).

On the other hand, the integrand of the leading shadowing correction (107), (21) is a smooth function of ρ . Furthermore, it is dominated by the contribution from large $\rho \sim R_p$. For this reason, it would be inappropriate to enforce the LLA limit of integration $\rho^2 > 1/Q^2$ in the shadowing correction (107). If, nonetheless, one goes ahead and does so, then differentiation in the first line of Eq. (107) will give

$$\begin{aligned} Q^2 \frac{\partial}{\partial Q^2} \left[Q^2 \Delta \sigma^{(sh)} \left(\rho^2 > \frac{1}{Q^2}, x, Q^2 \right) \right] \\ \propto \frac{1}{Q^2 B_{3\text{IP}}} [Q^2 \sigma(1/Q)]^2 \\ \propto \frac{1}{Q^2 B_{3\text{IP}}} \alpha_S(Q^2)^2 [xg(x, Q^2)]^2. \end{aligned} \quad (126)$$

The familiar form of the GLR nonlinear shadowing correction to the GLDAP equation for the density of gluons,¹⁹

$$Q^2 \frac{\partial}{\partial Q^2} [x \Delta g^{(sh)}(x, Q^2)] \\ \propto \frac{\alpha_s(Q^2)^2}{Q^2 B_{3IP}} \int_x^{y_m} \frac{dy}{y} [y g(y, Q^2)]^2, \quad (127)$$

is different from our result (108), (94). Evidently, neglecting the contribution to the shadowing term from $\rho^2 < 1/Q^2$ and/or the $\propto 1/Q^2$ corrections to the leading form of the wave function in Eqs. (21) and (107) cannot be justified, which makes the GLR equation highly questionable. It is interesting to note that Mueller and Qiu²⁰ had already expressed, but did not elaborate on and did eventually dismiss, similar doubts about the validity of the GLR nonlinear equation (see also the recent preprint by Levin and Wüsthoff²¹). The GLR term is a part of the $\propto 1/Q^2$ corrections to the leading shadowing term given by our Eq. (108); see also the above discussion on the fusion of partons in Section 7.5.

8. CONCLUSIONS AND DISCUSSION

Our principal conclusion is that diffraction dissociation of virtual photons in DIS can be described as DIS on pomerons with a well-defined and GLDAP-evolving structure function. Furthermore, we have shown that such a description persists beyond the single-pomeron exchange approximation. Our new result is that we have identified the valence $q\bar{q}$, the valence glue and the sea $q\bar{q}$ parton distributions in the pomeron, which are to be used as an input in the QCD evolution of the pomeron structure function. We have found that the normalization of the valence glue and sea in the pomeron is fixed by the single dimensional coupling A_{3IP}^* , which is sensitive to the infrared regularization. Our principal finding is that this coupling A_{3IP}^* (and the corresponding triple-pomeron coupling $A_{3IP}(Q^2)$, which we have shown only weakly depends on Q^2) must be approximately equal to the triple-pomeron coupling $A_{3IP}(0)$ as measured in the diffraction dissociation of real photons.³¹ This approximate equality $A_{3IP}^* \approx A_{3IP}(0)$ was conjectured long ago³⁰ and has been a basis of the successful phenomenology of nuclear shadowing in DIS.^{23,24,36} This equality was also used in the prediction⁷ of the rate of diffraction dissociation in DIS, which is in good agreement with the first data by the ZEUS collaboration.³² An important implication of separation of the infrared-sensitive input structure function of the pomeron from the hard QCD evolution effects is that jet activity in DIS on the pomeron must be similar to that in DIS on the proton.

We have derived the unitarity (shadowing) correction to the proton structure function at small x , and have demonstrated that the unitarized structure function satisfies the conventional, linear, GLDAP evolution equations. We emphasize the intrinsic simplicity of our light-cone s channel formalism used in this derivation. Firstly, our formalism implements in a very simple way the color gauge invariance constraints. Secondly, exact factorization of the photoabsorption cross section into the wave function and (multiparticle) dipole cross section allows an easy identification of the partial waves of the dipole cross section as

an object of the s channel unitarization. Thirdly, we took full advantage of the diagonalization of the scattering matrix as a function of the transverse separation and longitudinal momenta of partons in the multiparton Fock states of the photon. This enabled us to easily impose the s -channel unitarization on the total cross sections of all multiparticle Fock states of the photon. This also enabled us to identify the constituent gluon wave function of the pomeron, which gives a very economic description of the shadowing process in terms of the single parameter A_{3IP}^* , which is under good control as it is related to the triple-pomeron coupling $A_{3IP}(0)$ known from real photoproduction experiments. We have shown how multipomeron exchanges in the shadowing structure function and in diffraction dissociation can be summed in a very compact form that only renormalizes the effective flux of pomerons in the proton.

One of the authors (NNN) would like to thank V. V. Anisovich and L. G. Dakhno for criticism and L. N. Lipatov for numerous discussions on the pomeron and deep inelastic scattering during the past years. We are grateful to V. Barone, M. Genovese, E. Predazzi and V. R. Zoller for useful comments and discussions.

- ¹ K. A. Ter-Martirosyan, Phys. Lett. **B44**, 179 (1973); A. B. Kaidalov and K. A. Ter-Martirosyan, Nucl. Phys. **B75**, 471 (1974).
- ² G. Ingelman and P. Schlein, Phys. Lett. **B152**, 256 (1985).
- ³ H. Fritzsch and K. H. Streng, Phys. Lett. **B164**, 391 (1985).
- ⁴ E. L. Berger, J. C. Collins, D. E. Soper, and G. Sterman, Nucl. Phys. **B286**, 704 (1987).
- ⁵ A. Donnachie and P. V. Landshoff, Phys. Lett. **B191**, 309 (1987); Nucl. Phys. **B303**, 634 (1988).
- ⁶ V. V. Abramovskii and R. G. Betman, Sov. J. Nucl. Phys. **49**, 1205 (1989).
- ⁷ N. N. Nikolaev and B. G. Zakharov, Z. Phys. **C53**, 331 (1992).
- ⁸ N. N. Nikolaev, in *Diffraction and Elastic Scattering*, Proc. Int. Conf. on Elastic and Diffractive Scattering, La Biodola, Isola d'Elba, Italy, 22–25 May 1991; Nucl. Phys. (Proc. Suppl.) **B25**, 152 (1992).
- ⁹ J. Bartels and G. Ingelman, Phys. Lett. **B235**, 175 (1990).
- ¹⁰ G. Ingelman and K. Prytz, Z. Phys. **C58**, 285 (1993).
- ¹¹ V. N. Gribov and L. N. Lipatov, Sov. J. Nucl. Phys. **15**, 438 (1972); L. N. Lipatov, Sov. J. Nucl. Phys. **20**, 181 (1974).
- ¹² Yu. L. Dokshitzer, Sov. Phys. JETP **46**, 641 (1977).
- ¹³ G. Altarelli and G. Parisi, Nucl. Phys. **B126**, 298 (1977).
- ¹⁴ E. M. Levin and M. G. Ryskin, Sov. J. Nucl. Phys. **34**, 619 (1981).
- ¹⁵ A. S. Pak, N. O. Sadykov, and A. V. Tarasov, Sov. J. Nucl. Phys. **42**, 619 (1985).
- ¹⁶ P. E. Volkovitski, A. M. Lapidus, V. I. Lysin, and K. A. Ter-Martirosyan, Sov. J. Nucl. Phys. **24**, 648 (1976); A. Capella and J. Kaplan, Phys. Lett. **B52**, 448 (1974).
- ¹⁷ A. Donnachie and P. V. L. Landshoff, Phys. Lett. **B296**, 227 (1992).
- ¹⁸ E710 Collaboration: N. A. Amos *et al.*, Phys. Lett. **B301**, 313 (1993).
- ¹⁹ L. V. Gribov, E. M. Levin, and M. G. Ryskin, Phys. Reports **C100**, 1 (1983).
- ²⁰ A. H. Mueller and J. Qiu, Nucl. Phys. **B268**, 427 (1986).
- ²¹ E. M. Levin and M. Wüsthoff, DESY 92-166 (1992).
- ²² B. Badelek, K. Charchula, M. Krawczyk, and J. Kwiecinski, Rev. Mod. Phys. **64**, 927 (1992).
- ²³ N. N. Nikolaev and B. G. Zakharov, Phys. Lett. **B260**, 414 (1991).
- ²⁴ N. N. Nikolaev and B. G. Zakharov, Z. Phys. **C49**, 607 (1991).
- ²⁵ J. D. Bjorken, J. Kogut, and D. E. Soper, Phys. Rev. **D3**, 1382 (1971).
- ²⁶ E. A. Kuraev, L. N. Lipatov, and V. S. Fadin, Sov. Phys. JETP **44**, 443 (1976); **45**, 199 (1977).
- ²⁷ Ya. Ya. Balitsky and L. N. Lipatov, Sov. J. Nucl. Phys. **28**, 822 (1978).
- ²⁸ L. N. Lipatov, Sov. Phys. JETP **63**, 904 (1986); L. N. Lipatov, Pomeron in Quantum Chromodynamics, in *Perturbative Quantum Chromodynamics*, A. H. Mueller (ed.), World Scientific, Singapore (1989).

- ²⁹N. N. Nikolaev, B. G. Zakharov, and V. R. Zoller, Jülich preprint KFA-IKP(TH)-1993-34, JETP Lett. **59**, 6 (1994).
- ³⁰N. N. Nikolaev, *EMC Effect and Quark Degrees of Freedom in Nuclei: Facts and Fancy*, Oxford Univ. Preprint OU-TP 58/84 (1984); Multi-quark Interactions and Quantum Chromodynamics, *Proc. VII Int. Seminar on Problems of High-Energy Physics*, 19–26 June 1984, Dubna, USSR.
- ³¹T. J. Chapin *et al.*, Phys. Rev. **D31**, 17 (1985).
- ³²ZEUS Collaboration: M. Derrick *et al.*, Phys. Lett. **B317**, 481 (1993).
- ³³V. Barone, M. Genovese, N. N. Nikolaev, E. Predazzi, and B. G. Zakharov, Torino Preprint DFTT 28/93, June 1993.
- ³⁴F. E. Low, Phys. Rev. **D12**, 163 (1975); S. Nussinov, Phys. Rev. Lett. **34**, 1286 (1975); J. F. Gunion and D. Soper, Phys. Rev. **D15**, 2617 (1977).
- ³⁵V. N. Gribov, Lund preprint LU TP 91-7 (1991).
- ³⁶V. Barone, M. Genovese, N. N. Nikolaev, E. Predazzi, and B. G. Zakharov, Z. Phys. **C58**, 541 (1993).
- ³⁷V. Barone, M. Genovese, N. N. Nikolaev, E. Predazzi, and B. G. Zakharov, Phys. Lett. **B304**, 176 (1993).
- ³⁸V. Barone, M. Genovese, N. N. Nikolaev, E. Predazzi, and B. G. Zakharov, Int. J. Mod. Phys. **A8**, 2779 (1993).
- ³⁹V. Barone, M. Genovese, N. N. Nikolaev, E. Predazzi, and B. G. Zakharov, Phys. Lett. **B268**, 279 (1991); **B317**, 433 (1993).
- ⁴⁰G. V. Frolov, V. N. Gribov, and L. N. Lipatov, Phys. Lett. **31**, 34 (1970); L. N. Lipatov and G. V. Frolov, Sov. J. Nucl. Phys. **13**, 333 (1971).
- ⁴¹Yu. L. Dokshitzer, D. I. Dyakonov, and S. I. Troyan, Phys. Rep. **C58**, 265 (1980).
- ⁴²N. N. Nikolaev, B. G. Zakharov, and V. R. Zoller, JETP, **105** (in press).
- ⁴³B. Z. Kopeliovich, N. N. Nikolaev, and I. K. Potashnikova, Phys. Rev. **D39**, 769 (1989).
- ⁴⁴ZEUS Collaboration: M. Derrick *et al.*, Phys. Lett. **B293**, 465 (1992); H1 Collaboration: T. Ahmed *et al.*, Phys. Lett. **B299**, 374 (1992).
- ⁴⁵B. G. Zakharov, Sov. J. Nucl. Phys. **49**, 860 (1989).
- ⁴⁶R. C. Arnold, Phys. Rev. **153**, 1523 (1967).
- ⁴⁷K. A. Ter-Martirosyan, Sov. J. Nucl. Phys. **10**, 600 (1970).
- ⁴⁸R. C. Arnold, Phys. Rev. **B136**, 1388 (1964).
- ⁴⁹T. T. Chou and C. N. Yang, Phys. Rev. **D19**, 3268 (1979); Phys. Lett. **B123**, 457 (1983); C. Bourelly, J. Soffer and T. T. Wu, Phys. Lett. **B121**, 284 (1983); Z. Phys. **C37**, 369 (1988).
- ⁵⁰V. N. Gribov, Sov. Phys. JETP **26**, 414 (1968).
- ⁵¹A. B. Kaidalov, Sov. J. Nucl. Phys. **13**, 226 (1971); Phys. Rep. **50**, 157 (1979).
- ⁵²NMC Collaboration: M. Arneodo *et al.*, Phys. Lett. **B309**, 222 (1993).
- ⁵³R. G. Roberts, *The Structure of the Proton. Deep Inelastic Scattering*, Cambridge University Press (Cambridge, 1990); Yu. L. Dokshitzer, V. A. Khoze, A. H. Mueller, and S. I. Troyan, *Basics of Perturbative QCD*, Editions Frontières Gif-sur-Yvette (1991).
- ⁵⁴N. N. Nikolaev and V. I. Zakharov, Phys. Lett. **B55**, 397 (1975); V. I. Zakharov and N. N. Nikolaev, Sov. J. Nucl. Phys. **21**, 227 (1975).

This article was published in English in the original Russian journal. It is reproduced here with the stylistic changes by the Translation Editor.